Spectroscopy of $^{188}_{82}Pb_{106}$: Evidence for shape coexistence

G. D. Dracoulis,[1] G. J. Lane,[1,2] A. P. Byrne,[1,3] T. Kibédi,[1] A. M. Baxter,[3] A. O. Macchiavèlli,[2] P. Fallon,[2] and R. M. Clark[2]
[1]*Department of Nuclear Physics, Australian National University, Canberra, ACT 0200, Australia*
[2]*Nuclear Science Division, Lawrence Berkeley National Laboratory, Berkeley, California, 94720, USA*
[3]*Department of Physics, The Faculties, Australian National University, Canberra, ACT 0200, Australia*
(Received 6 February 2004; published 26 May 2004)

In-beam γ-ray spectroscopy of ^{188}Pb has been carried out using Gammasphere. Time-correlated γ-γ coincidence methods have allowed the identification of new structures above and below the two-particle isomeric states. The detailed decay of the proposed $K^{\pi}=8^{-}$, 1 μs isomer has been established, together with a rotational band based on the isomer. Both decay and band properties confirm the association with a prolate deformation and the two-quasineutron $9/2^{+}[624]\otimes 7/2^{-}[514]$ configuration. The band structure identified above the 11^{-} isomer from the two-proton configuration $9/2^{-}[505]\otimes 13/2^{+}[606]$ has a moment of inertia similar to those of the bands known in heavier isotopes and to the one-quasiproton components, but the perturbations and in-band properties are not as expected for a simple, symmetric oblate deformation. This structure is fed by a (19^{-}) isomer. Possible configurations for this and other multiquasiparticle states are discussed in the context of multi-quasiparticle calculations for coexisting deformations. Low-spin structures populated partly from the decay of the 8^{-} isomer have also been identified. Several of these may be associated with proposed excited 0^{+} states. Their properties, including yrare-yrast $E0$ decays and gamma-ray branching ratios, are analyzed using band-mixing models. These and other analyses support a shape coexistence scenario, with some qualifications.

DOI: 10.1103/PhysRevC.69.054318 PACS number(s): 27.70.+q, 23.20.Lv, 21.10.Re, 25.70.Gh

I. INTRODUCTION

The nucleus ^{188}Pb was the first of the very neutron-deficient Pb nuclei for which the presence of a prolate-deformed rotational band coexisting with the expected spherical configurations, was proposed [1]. Since that time there has been extensive activity in their study, aided by developments in spectroscopic techniques.

Theoretical interest in nuclei which exhibit coexisting shapes arises partly because the phenomenon is controlled by inhomogeneities in the single-particle level densities near the Fermi surface. Prediction of such multiple shapes is therefore a sensitive test of nuclear potentials, as well as of residual interactions such as pairing, and thus bears on the validity of mean-field theories and general methods for estimating the stability of heavy nuclei.

The situation in Pb nuclei, with a closed $Z=82$ proton shell, has parallels with the $Z=80$ (Hg) nuclei, in which shape coexistence was observed nearly three decades ago. The manifestations in Hg included unexpected values of charge radii and magnetic moments in the odd-neutron isotopes [2,3] and anomalies in the spacing of the yrast (lowest energy state for a given spin) sequences in the even-even isotopes at low spin, attributed to the crossing of collective bands arising from each subminimum. These effects were taken to be indicative of a secondary prolate-deformed minimum in the potential well, lying only a few hundred keV above the mercury ground states, which were believed to be weakly oblate in deformation [4,5]. In microscopic terms, the subminima in the potential wells are related to "intruder" configurations arising from occupation of orbitals which lie above the $Z=82$ closed shell at sphericity, but which can be accessed at a low cost in energy at large prolate or oblate deformations.

A more complicated and spectroscopically rich situation will occur at $Z=82$, where similar deformed shapes are expected, but with the intrusion of a deep spherical mimimum. Spherical configurations naturally dominate the ground and excited state structures in Pb nuclei near the $N=126$ closed neutron shell, but if a substantial number of neutrons are removed, *three* potential minima, spherical, oblate, and prolate, are calculated to occur, all at low energies. The early Nilsson-Strutinsky calculations of potential energy surfaces (PES) by May, Pashkevich, and Frauendorf [6] and more recently those of Bengtsson and Nazarewicz [7,8] predicted that the prolate subminimum would have a parabolic energy dependence on neutron number with its minimum near mid-shell, $N\sim 104$ (^{186}Pb), and this seems to be borne out, at least superficially in terms of energy systematics.

As can be implied from the recent systematics [9–11], excited states from each predicted deformation, prolate, spherical, and oblate, might compete near $N=106$ and 108, and the ideal situation would be to characterize the minima through identification of the excitations or collective modes within each minimum. As implied from the discussion above, this is a somewhat simplistic aim in that such excitations will only exist if the minima are distinct, a situation that is more likely to pertain for higher spins, or more precisely, for higher-K values. Nevertheless, to the extent that it can be quantified, mixing itself is of interest since it contains information on the detailed shape of the nuclear potential and the dynamics.

The experimental challenge caused by the complex spectroscopic situation is amplified by the fact that the nuclei are very neutron deficient, and will have key excited states that are likely to be non-yrast and therefore difficult to populate.

II. EXPERIMENTAL BACKGROUND

Despite recent technical advances, spectroscopic information in the region remains fragmentary, largely because of unavoidable experimental limitations. For example, while α-decay studies provide a powerful means of isolating excited 0^+ states, which may be evidence for the presence of different intrinsic structures, that selectivity is at the expense of the population of other excited states. Further, formation of the very neutron-deficient Po parents is itself difficult. In-beam spectroscopy is more direct and usually more prolific, but for neutron-deficient heavy nuclei it becomes severely limited because of the competition from fission. It is also less favorable for the population of nonyrast states. Recoil-decay tagging techniques overcome some of the sensitivity limitations, leading to many of the recent results on the very neutron-deficient cases (as reviewed in Ref. [11]), but recoil techniques can be compromised by the presence of isomers which are likely to be present as a characteristic feature of the nuclear structure [12].

The current experimental situation near $N=106$ is that evidence for a triple shape coexistence has been claimed [13] for $^{186}Pb_{104}$ in the form of the observation of the ground state and two excited 0^+ states at low energy (532 and 650 keV). While the presence of 0^+ states is not in itself a measure of differing deformations, configuration differences are argued for, in this case, on the basis of contrasting α-decay widths from the decay of ^{190}Po. The only other states known in ^{186}Pb are those forming the yrast sequence up to spin 14^+ with states above spin 2^+ being attributed to the prolate band [14,15]. Association of this sequence with prolate deformation is largely on the basis of the similarity of its moment of inertia to other bands, a common assumption in this region.

In $^{190}Pb_{108}$, considerably more experimental information is available [9] but the prolate band has apparently risen in energy sufficiently that the yrast spectrum is dominated by the spherical and oblate structures, including microsecond isomers from 11^- (oblate) and 12^+ (spherical) configurations, although a candidate prolate band has been proposed [9]. One excited 0^+ state, at 658 keV, is known and interpreted as being of oblate deformation [16,17].

In the intervening case of $^{188}Pb_{106}$ the yrast sequence is again formed mainly by the proposed prolate band which is known up to spin 16^+, but the presence of 8^-, 11^-, and 12^+ isomeric two-quasiparticle states found near the yrast line has been proposed recently as a manifestation of triple shape coexistence [10]. That study also identified a number of nonyrast states populated in the decay of the 8^- isomer itself [10]. The situation regarding excited 0^+ states in ^{188}Pb is not clear. Initially the α-decay fine structure from ^{192}Po which identified excited 0^+ states at 568(4) keV and 767(12) was analyzed in detail to relate mixing in both the Po parent and the Pb daughter [18], giving constraints on the mixing between specific states in ^{188}Pb and the magnitude of the mixing matrix elements. However, the higher of these states has not been confirmed in the most recent α-decay work (as will be discussed later).

In the measurements reported here, extensive new information has been obtained, both on the isomeric states and their associated collective structures, and on low-lying low-spin states which could be associated with excited 0^+ states. Some constraints can therefore be placed on possible branches to such states and therefore on their excitation energies. (Some of these results have been partially reported [19–21].)

III. EXPERIMENTAL CONSIDERATIONS

The first aim of the new experiments was to identify the structures above each of the intrinsic excitations proposed in ^{188}Pb, by exploiting time correlations and multiple energy gating to gain sensitivity. The second aim was to categorize as completely as possible the decay of the proposed 8^- isomer and thus establish its character and that of the low-spin states in its decay path. Possible connections to the proposed excited 0^+ states were to be sought, as well as identification of other states and excitations.

IV. EXPERIMENTAL DETAILS

Gammasphere with 101 Compton suppressed detectors was used to measure three- and higher-fold γ-γ-time coincidences. Approximately 2.3×10^9 valid events were recorded. The nuclei were produced in the ^{156}Gd(^{36}Ar,$4n$)^{188}Pb reaction with 174 MeV beams provided by the 88-Inch Cyclotron operated by the Lawrence Berkeley National Laboratory. The nuclei were stopped in a gold backing at the target position and particular attention was paid to the measurement and analysis of the time information. The ±700 ns acceptance allowed correlation across the isomers whose mean lives range from 38 ns to 1.2 μs. For orientation it should be noted that the cross section for production of ^{188}Pb is of the order of 10 mb, in the presence of similar cross sections for the channels which involve the emission of a proton or α particle, a fission cross section of several hundred mb, and a high radioactivity flux due to the need to stop all nuclei at the target position. Population of the 8^- isomer is less than 1% of that of the 2^+ yrast state with a correspondingly low population of the states above.

A. Analysis methods

Recent developments in software [22] allowed the fast production of matrices with different time and gating γ-ray conditions. With the resulting flexibility, a variety of time conditions relating both the time difference between specific γ rays, and their time relative to the beam pulses, was used to provide high sensitivity for identifying γ rays which otherwise would be lost in the background of competing reactions. This allowed selection and separation of different parts of the level scheme, thus reducing ambiguities.

1. Gamma-gamma time correlations

Given the limited time between beam pulses (70 ns from the cylotron period) and the need to optimize yield, particular care was taken in the analysis to match the times for all 101 detectors across the complete time range.

The matrices constructed included a γ-γ-γ cube with the time-difference condition of ±30 ns and a γ-γ-γ cube with

TABLE I. Total conversion coefficients for selected transitions in ^{188}Pb compared to theoretical values.

E_γ (keV)	α_T	Theory[a]			Assignment
		$E1$	$M1$	$E2$	
yrare-yrast					
431.7	~0.3	0.0132	0.169	0.0427	$E0/E2$
352.6	1.3(3)	0.0205	0.290	0.073	$E0/E2$
250.8	2.4(3)	0.0453	0.736	0.203	$E0/E2$
228.7	2.9(5)	0.0565	0.949	0.274	$E0/E2$
8^- isomer					
103.0	8(2)	0.410	9.12	5.69	$M1/E2$
129	2.0(13)	0.234	4.78	2.24	$E2$
278.2	0.08(5)	0.0356	0.556	0.147	$E1$
360.2	<0.05	0.0197	0.275	0.069	$E1$
(19^-) isomer					
217.8	0.23 or 0.51	0.0637	1.09	0.323	$E2$

[a]Reference [23].

the same time-difference condition, but with absolute time constraints to select transitions in 40-ns-wide intervals between the beam pulses and encompassing the total delayed time region of 15 to 700 ns accepted in the Gammasphere.

Other general data arrays included γ-γ matrices with the ±30 ns time condition and more restricted out-of-beam regions of 15–20, 120–300, and 300–700 ns, as well as early-delayed γ-γ matrices with related time conditions but with transitions above and below isomers selected, in some cases with energy gates to isolate specific isomers.

A substantial part of the primary analysis was carried out on γ-γ matrices with a ±30 ns time condition and an additional gate on either the 724 keV $2^+ \rightarrow 0^+$ transition or on the 953 keV $2^{+\prime} \rightarrow 0^+$ transition (as identified in this work), thus providing channel selection on ^{188}Pb. Subsequently, various γ-γ matrices were constructed including one with energy gates on the 340, 370, 434, 499, and 724 keV yrast transitions delayed by 15–300 ns. In this case, an equivalently gated matrix in the 300–700 ns region was subtracted, so as to isolate further, pairs of transitions feeding the relatively short 11^- and 12^+ isomers. Similarly a γ-γ matrix was constructed with gates on clean transitions and delayed time to select pairs of transitions feeding the 1.1 μs 8^{-1} isomer. (This case was more difficult because of the fragmented decay of this isomer, and its relatively long lifetime.)

2. Angular distributions

In order to obtain angular distribution information, the data collected in the three rings of the Gammasphere were separated, corresponding to angles (averaged in $\cos^2\theta$) of 30°, 53°, and 76°, and spectra were constructed with time and energy gates similar to those used for the matrices described earlier. The majority of this analysis, which involved peak-area extraction and subsequent fitting to obtain the coefficient A_2/A_0 (assuming $A_4=0$) was carried out for the sets of three spectra constructed with the following conditions:

(a) prompt (±30 ns) single gate on the 724 keV transition,

(b) prompt double gate on the 724 and 340 keV transitions,

(c) prompt double gate on the 724 and 370 keV transitions,

(d) prompt (±30 ns) single gate on the 953 keV transition,

(e) delayed (15-300 ns)) gate on the 340, 370, 434, 499, 724 keV transitions following the decay of the 11^- and 12^+ isomers,

(f) delayed (120–700 ns) gate on 340, 360, 362, 429, 472, 724, 783, and 953 keV transitions which follow the decay of the 8^- isomer.

Set (e), for example, isolates the transitions above the 11^- and 12^+ isomers, effectively removing complications from contaminants and accidental energy coincidences.

3. Total conversion coefficients

In the case of relatively low energy transitions, total conversion coefficients were estimated from intensity balances in selected delayed spectra and/or using spectra with double gates on transitions directly feeding a particular state, or alternatively with gates above and below the transition path of interest. The results for the 335 and 344 keV transitions which directly depopulate the 38 ns and 136 ns isomers confirm the analysis presented previously [10]. Other results are collected in Table I including limits for the 218 keV transition, which directly depopulates the isomer (now established) at 4783 keV and, with the resolution of the decay paths for all branches from the 8^- isomer at 2577 keV, measurements for the 103, 129, 278, and 360 keV transitions from that isomer. Values were also obtained for transitions between the yrast and yrare positive parity bands in which $E0$ components are proposed, as will be discussed in the following subsection.

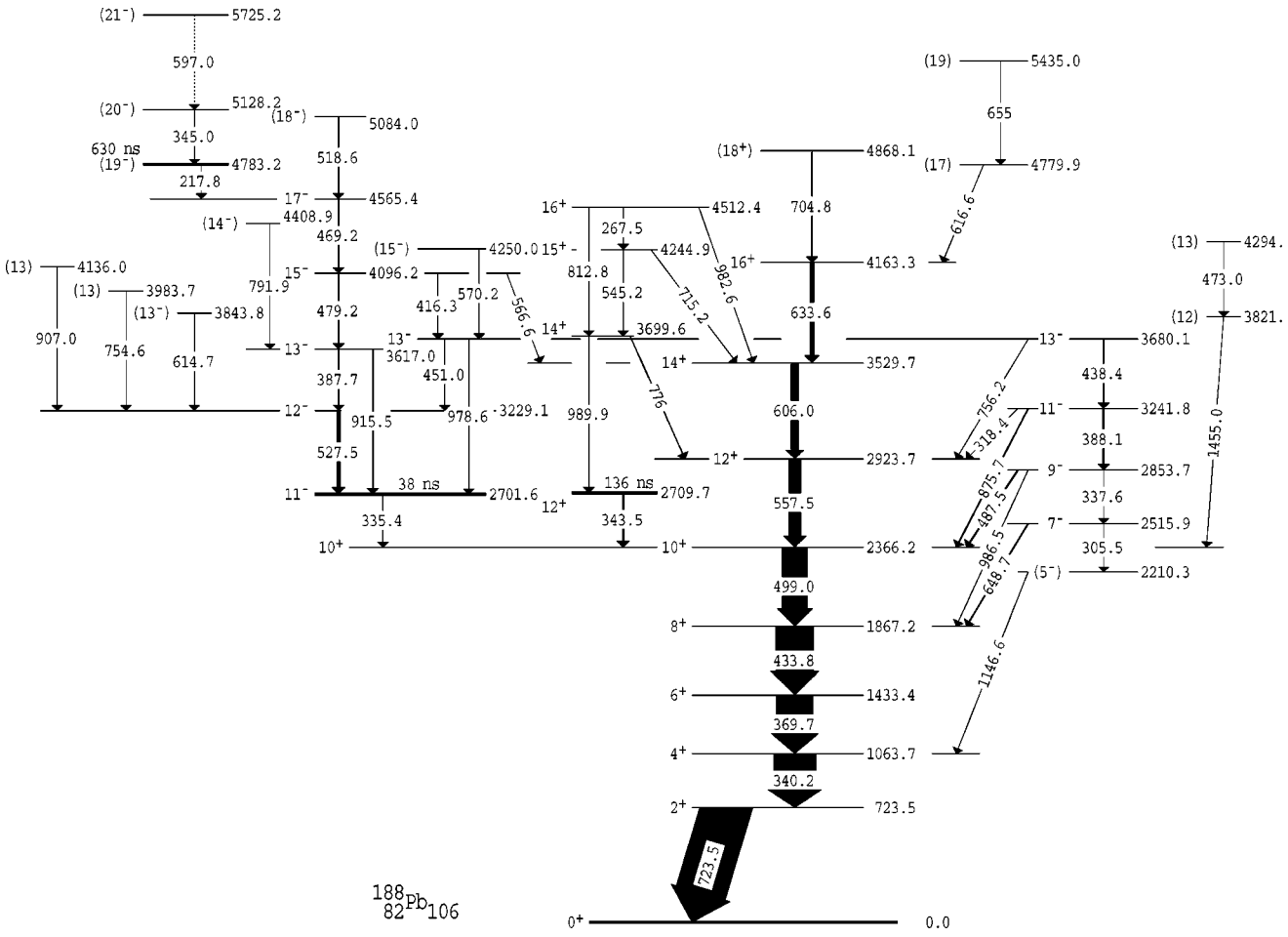

FIG. 1. Level scheme of ^{188}Pb in two parts; part I.

V. LEVEL SCHEME

The level scheme deduced for ^{188}Pb, incorporating about 50 new states, is shown in two parts in Figs. 1 and 2. Transitions assigned to ^{188}Pb are given in Table II together with approximate intensities and angular distribution information where available. Figure 1 shows the yrast sequence and levels connected either directly or indirectly to the 11^- and 12^+ isomers.

Figure 2 shows the 8^- isomer and its associated band, and the states to which it decays, as well as states based on them. Except for the common yrast sequence, and the tentatively assigned 380 keV transition from the 2853.7 keV state, (see the extreme left of Fig. 2. No connections between the two parts of the scheme have been observed).

Figure 3 shows double-gated spectra which illustrate the population pattern through low-lying states; the upper panel selects the main transitions proceeding through the 4^+ and 2^+ yrast states and the lower panel, the relatively weak path through the $4^{+\prime}$ and $2^{+\prime}$ states (double gate on the 362 and 953 keV transitions).

In this, and the subsequent discussion, references to transition energies and state energies are rounded off to the nearest kilovolt unless there is the possibility of ambiguity or need to identify states in the level scheme, in which case, more precise energies are quoted.

A. Level, spin, and parity assignments

1. 11^- and 12^+ isomers and associated states

No new branches were observed from the known isomers at 2702 and 2710 keV, but on the basis of other information, their character has been inverted compared to the original assignment [10]. That is, the 2702 keV, 38 ns mean life isomer is now assigned as 11^- while the 2710 keV, 136 ns isomer is assigned as 12^+. Previously the only spectroscopic information was a restriction on the total conversion coefficients for the 335 and 344 keV transitions required to balance the sum of the delayed intensity into the 10^+ yrast state [10]. This favored a combination of $E1$ and $E2$ or $E2$ and $E1$ for the 335 and 344 lines, respectively, both of which feed the 10^+ state. The higher relative strength of the 335 keV line was the argument used to favor $E2$ multipolarity and a tentative 12^+ assignment for the 2702 keV state, making the 2710 keV state 11^- by default.

However, the new angular distribution information for the 335 and 344 keV transitions (Table II) suggests dipole character for the 335 keV transition and quadrupole for the 344 keV transition, thus favoring the alternative spins and parities. This alone would be sufficient to choose the alternative assignment but the rearrangement is also strongly supported by the character of the collective structure above the

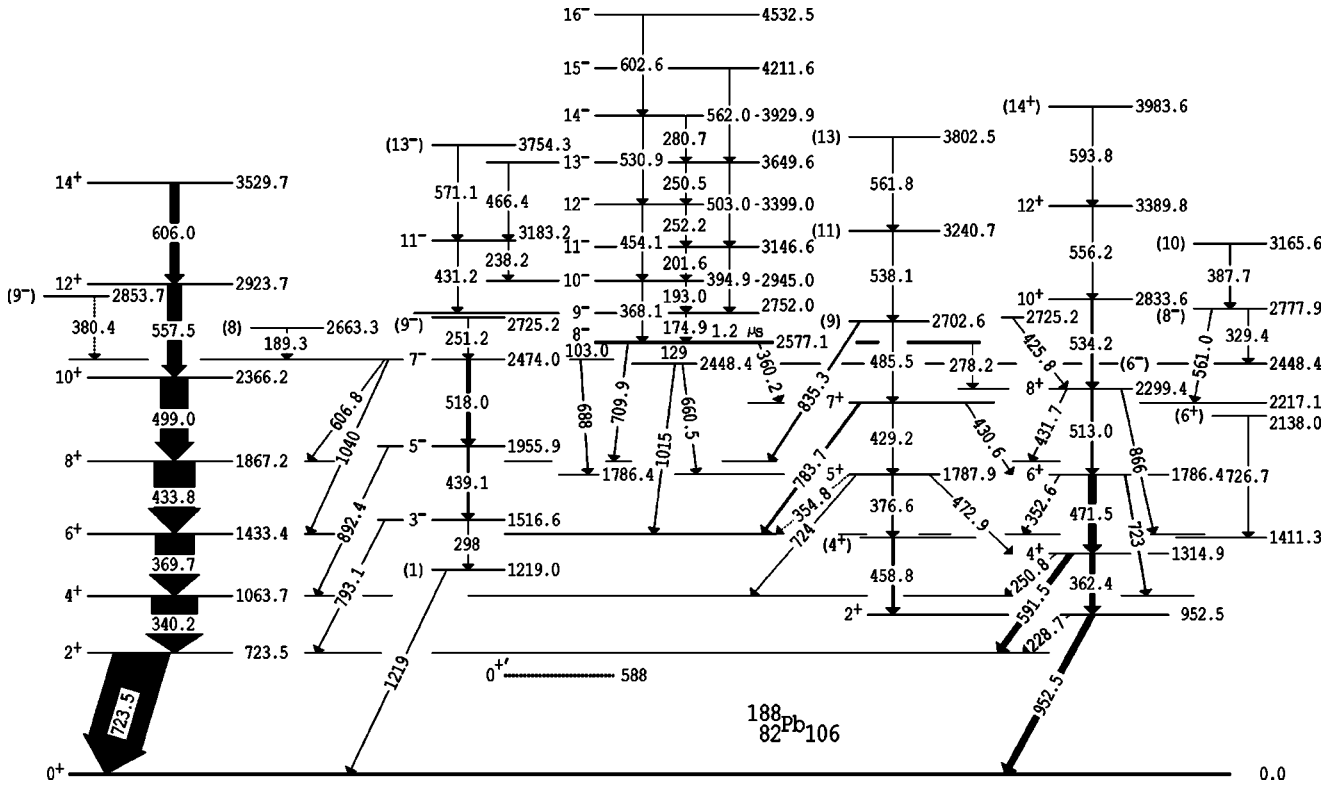

FIG. 2. Level scheme of ^{188}Pb in two parts; part II.

2702 keV state, which closely resembles the structures above the 11^- isomers in the heavier even-even isotopes, while the fragmented structure above the 2710 keV state is consistent with that above the known 12^+ isomers.

The validity of the original population argument depends crucially on the disposition of higher states (unknown at the time). As can be seen from the new level scheme shown in Fig. 1, the 11^- band is strongly fed by a (19^-) yrast isomer, which preferentially decays to the 11^- band, while the states above the 12^+ isomer also decay directly to the ground state band, thus depleting the 12^+ isomer of population. Both effects will distort any simple population argument. (It should also be noted that loss of cross section to fission limits the spin input, and therefore the entry region is unlikely to extend significantly past the highest states identified near spin $20\hbar$, hence their population is unlikely to be purely statistical.)

The main transitions above these isomers were assigned from time-correlated spectra such as that in Fig. 4. The lowest panel shows transitions preceding in time the 499 keV 10^+ to 8^+ transition, while the upper two panels show equivalent gates on the primary transitions from the two isomers.

Development of the scheme above the 11^- and 12^+ isomers proceeded from analyses of the prompt γ-γ coincidences projected from the matrix constructed with delayed gates on transitions following the isomers. The lowest panel of Fig. 5 shows the gate on the 469 keV transition, illustrating the main transitions in the sequence above the 11^- state, as well as the 218 keV transition which is a direct decay from the higher-lying isomer at 4783 keV. Transitions above that isomer were then isolated by gating on transitions in the main 11^- sequence requiring that these were delayed with respect to the primary transitions, and that all were above the delayed transitions following the decay of the 11^- isomer.

The isomer at 4783 keV was implied from the earlier work [10] but was neither precisely placed, nor was a lifetime established, although it was suggested to be in the 0.5 to 1 μs region. A mean life of 630(80) ns has been deduced from the present data from the delayed intensities in the transitions of the 11^- band. These were obtained by constructing γ-γ-γ cubes in contiguous delayed time regions, with additional gates to select transitions which precede the 11^- isomer decay, and using double gating within the band to eliminate remaining contaminants.

The anisotropy information for the transitions above the 11^- isomer (see Table II) shows that the 528 and 388 keV transitions have very large negative A_2/A_0 coefficients indicating mixed $M1/E2$ dipoles, while the 916 keV transition crossover has the characteristics of a stretched quadrupole, leading directly to the 12^- and 13^- assignments for the 3229 and 3617 keV states. Similarly, the properties of the 451 and 979 keV transitions lead to the assignment of a second 13^- state at 3680 keV. Both 479 and 416 keV decays from the 4096 keV state to the two 13^- states have stretched quadrupole properties, leading to assignment of $J^\pi = 15^-$ to the 4096 keV state, which also has a branch to the 14^+ yrast state. The 469 keV transition appears to be quadrupole suggesting 17^- for the 4565 keV state, while the 519 keV transition which feeds it, is apparently a dipole. The fact that a regular sequence ($\Delta J = 1$ or $\Delta J = 2$) is not observed is partly explained by a crossing with the negative parity band seen on the right of Fig. 1. The 3680 keV state is a member of that

TABLE II. Engergies, approximate intensities, angular distributions, and initial and final energies, spins, and parities of transitions assigned to ^{188}Pb.

E_γ[a]	I_γ[b]	A_2/A_0	E_i	E_f	J_i^π	J_f^π
103.0	20(3)		2577.1	2474.0	8^-	7^-
129	21(3)		2577.1	2448.4	8^-	(6^-)
174.9	67(6)	−0.63(18)	2752.0	2577.1	9^-	8^-
189.3	20(6)		2663.3	2474.0	(8)	7^-
193.0	51(5)	−0.72(17)	2945.0	2752.0	10^-	9^-
201.6	28(5)		3146.6	2945.0	11^-	10^-
217.8	30(4)	+0.33(29)	4783.2	4565.4	(19^-)	17^-
228.7	52(4)	−0.33(15)	952.5	723.5	2^+	2^+
238.2	21(4)	−0.8(3)	3183.2	2945.0	11^-	10^-
250.5	12(3)	−0.5(3)	3649.6	3399.0	13^-	12^-
250.8	59(5)	−0.31(18)	1314.9	1063.7	4^+	4^+
251.2	30(9)		2725.2	2474.0	(9^-)	7^-
252.2	13(3)		3399.0	3146.6	12^-	11^-
267.5	96(20)	−0.39(20)	4512.4	4244.9	16^+	15^+
278.2	70(3)		2577.1	2299.4	8^-	8^+
280.7	∼7		3929.9	3649.6	14^-	13^-
298	60(15)		1516.6	1219.0	3^-	(1^-)
305.5	∼15		2515.9	2210.3	7^-	(5^-)
318.4	37(8)		3241.8	2923.7	11^-	12^+
329.4	40(6)		2777.9	2448.4	(8^-)	(6^-)
335.4	443(21)	−0.16(8)	2701.6	2366.2	11^-	10^+
337.6	28(4)		2853.7	2515.9	9^-	7^-
340.2	4190(65)	+0.24(4)	1063.7	723.5	4^+	2^+
343.5	232(18)	+0.18(11)	2709.7	2366.2	12^+	10^+
345.0	∼10		5128.2	4783.2	(20^-)	(19^-)
352.6	42(7)		1786.4	1433.4	6^+	6^+
354.8	34(10)		1787.9	1433.4	5^+	6^+
360.2	148(5)		2577.1	2217.1	8^-	7^+
362.4	503(14)	+0.16(14)	1314.9	952.5	4^+	2^+
368.1	34(7)	+0.29(20)	2945.0	2577.1	10^-	8^-
369.7	3586(60)	+0.26(4)	1433.4	1063.7	6^+	4^+
376.6	139(18)	+1.0(4)	1787.9	1411.3	5^+	(4^+)
(380.4)	∼33		2853.7	2474.0	9^-	7^-
387.7	91(4)	−0.42(9)	3617.0	3229.1	13^-	12^-
387.7	16(3)		3165.6	2777.9	(10)	(8^-)
388.1	198(20)		3241.8	2853.7	11^-	9^-
394.9	24(5)		3146.6	2752.0	11^-	9^-
416.3	75(9)	+0.31(16)	4096.2	3680.1	15^-	13^-
425.8	12(3)		2725.2	2299.4	(9^-)	8^+
429.2	360(40)		2217.1	1787.9	7^+	5^+
430.6	77(10)		2217.1	1786.4	7^+	6^+
431.2	25(5)	(∼0.3)	3183.2	2752.0	11^-	9^-
431.7	29(4)		2299.4	1867.2	8^+	8^+
433.8	3745(60)	+0.26(4)	1867.2	1433.4	8^+	6^+
438.4	132(15)		3680.1	3241.8	13^-	11^-
439.1	129(12)	+0.29(20)	1955.9	1516.6	5^-	3^-
451.0	69(4)	−0.48(12)	3680.1	3229.1	13^-	12^-
454.1	35(5)		3399.0	2945.0	12^-	10^-

TABLE II. (*Continued.*)

E_γ [a]	I_γ [b]	A_2/A_0	E_i	E_f	J_i^π	J_f^π
458.8	239(15)	+0.23(14)	1411.3	952.5	(4^+)	2^+
466.4	21(3)		3649.6	3183.2	13^-	11^-
469.2	121(5)	+0.16(10)	4565.4	4096.2	17^-	15^-
471.5	667(15)	+0.24(10)	1786.4	1314.9	6^+	4^+
472.9	138(6)		1787.9	1314.9	5^+	4^+
473.0	~10		4294.0	3821.0	(13)	(12)
479.2	121(5)	+0.26(9)	4096.2	3617.0	15^-	13^-
485.5	120(6)		2702.6	2217.1	(9)	7^+
487.5	165(20)		2853.7	2366.2	9^-	10^+
499.0	2507(45)	+0.26(4)	2366.2	1867.2	10^+	8^+
503.0	18(4)		3649.6	3146.6	13^-	11^-
513.0	151(5)	(+0.21(9))	2299.4	1786.4	8^+	6^+
518.0	301(16)	+0.33(13)	2474.0	1955.9	7^-	5^-
518.6	59(4)	−0.21(16)	5084.0	4565.4	(18^-)	17^-
527.5	340(10)	−0.63(5)	3229.1	2701.6	12^-	11^-
530.9	21(5)		3929.9	3399.0	14^-	12^-
534.2	157(13)	+0.31(5)	2833.6	2299.4	10^+	8^+
538.1	67(3)		3240.7	2702.6	(11)	(9)
545.2	53(4)	−0.13(19)	4244.9	3699.6	15^+	14^+
(546)	~20			3843.8		(13^-)
556.2	43(6)		3389.8	2833.6	12^+	10^+
557.5	1224(30)	+0.37(6)	2923.7	2366.2	12^+	10^+
561.0	64(5)		2777.9	2217.1	(8^-)	7^+
561.8	24(5)		3802.5	3240.7	(13)	(11)
562.0	20(6)		4211.6	3649.6	15^-	13^-
566.6	16(3)		4096.2	3529.7	15^-	14^+
570.2	53(6)	+0.15(26)	4250.0	3680.1	(15^-)	13^-
571.1	30(5)		3754.3	3183.2	(13^-)	11^-
591.5	498(19)	+0.39(10)	1314.9	723.5	4^+	2^+
593.8	30(10)		3983.6	3389.8	(14^+)	12^+
597.0	~7		5725.2	5128.2	(21^-)	(20^-)
602.6	10(3)		4532.5	3929.9	16^-	14^-
606.0	754(38)	(+0.22(10))	3529.7	2923.7	14^+	12^+
606.8	~20		2474.0	1867.2	7^-	8^+
614.7	69(6)	−0.4(2)	3843.8	3229.1	(13^-)	12^-
616.6	~40		4779.9	4163.3	(17)	16^+
633.6	226(28)	+0.36(16)	4163.3	3529.7	16^+	14^+
648.7	105(20)		2515.9	1867.2	7^-	8^+
655	~5		5435.0	4779.9	(19)	(17)
660.5	120(20)		2448.4	1787.9	(6^-)	5^+
688	~10		2474.0	1786.4	7^-	6^+
704.8	41(8)		4868.1	4163.3	(18^+)	16^+
709.9	61(3)		2577.1	1867.2	8^-	8^+
715.2	70(8)		4244.9	3529.7	15^+	14^+
723	89(25)		1786.4	1063.7	6^+	4^+
723.5	**5000**		723.5	0.0	2^+	0^+
724	~20		1787.9	1063.7	5^+	4^+
726.7	26(5)		2138.0	1411.3	(6^+)	(4^+)

TABLE II. (*Continued.*)

E_γ [a]	I_γ [b]	A_2/A_0	E_i	E_f	J_i^π	J_f^π
754.6	32(6)		3983.7	3229.1	(13)	12^-
756.2	30(7)		3680.1	2923.7	13^-	12^+
776	33(7)		3699.6	2923.7	14^+	12^+
783.7	198(18)	1.0(2)	2217.1	1433.4	7^+	6^+
791.9	32(6)		4408.9	3617.0	(14^-)	13^-
793.1	177(24)	−0.16(32)	1516.6	723.5	3^-	2^+
812.8	27(8)		4512.4	3699.6	16^+	14^+
835.3	120(20)		2702.6	1867.2	(9)	8^+
866	13(4)		2299.4	1433.4	8^+	6^+
875.7	75(15)		3241.8	2366.2	11^-	10^+
892.4	240(20)	−0.11(16)	1955.9	1063.7	5^-	4^+
907.0	18(3)		4136.0	3229.1	(13)	12^-
915.5	155(7)	+0.22(9)	3617.0	2701.6	13^-	11^-
952.5	554(15)		952.5	0.0	2^+	0^+
978.6	53(4)	+0.31(20)	3680.1	2701.6	13^-	11^-
982.6	28(8)		4512.4	3529.7	16^+	14^+
986.5	62(7)		2853.7	1867.2	9^-	8^+
989.9	128(7)	+0.32(12)	3699.6	2709.7	14^+	12^+
1015	42(6)		2448.4	1433.4	(6^-)	6^+
1040	~60		2474.0	1433.4	7^-	6^+
1146.6	44(7)		2210.3	1063.7	(5^-)	4^+
1219	~40		1219.0	0.0	(1^-)	0^+
(1455)	(10)		3821.0	2366.2	(12)	10^+

[a]Energies with decimal place accurate to ~0.3 keV.
[b]Normalized to 1000 units for the $2^+ \rightarrow 0^+$ transition.

band that has been perturbed by mixing with the 13^- state from the 11^- band. This will be discussed further below.

The 615 keV transition evident in Fig. 4 directly feeds the 3229 keV state, thus establishing a state at 3844 keV, and a 546 keV transition may feed it but this is uncertain. The angular distribution of the 615 keV γ-ray also shows a large negative anisotropy, suggesting a mixed $M1/E2$ transition and therefore spin and parity 13^- for the initial state. (Note that several strong 615 keV transitions are present from competing reaction products.) Distribution information was not obtained for the 755 and 907 keV transitions, which are also single feeds into the 3229 keV state.

The 4783 keV isomeric state decays directly to the 4565 keV 17^- state via the 218 keV transition, and no other branches from the isomer have been identified. The value of

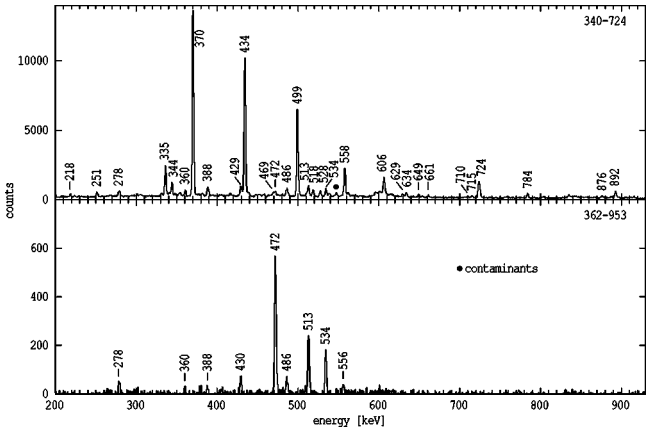

FIG. 3. Double-gated spectra with a prompt relative time condition but taken over all times, showing the transitions feeding through the 4^+ yrast state (upper panel) and through the yrare 4^+ and 2^+ states (lower panel). Only the main transitions are labeled.

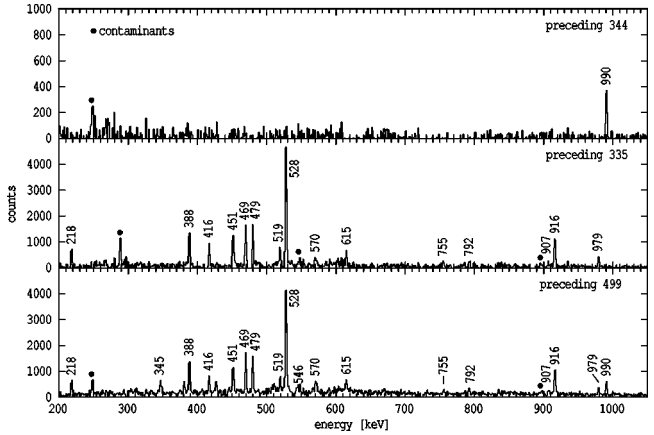

FIG. 4. Time-correlated spectra showing the transitions preceding in time, the individual gamma-rays indicated. Contaminants are labeled with filled circles.

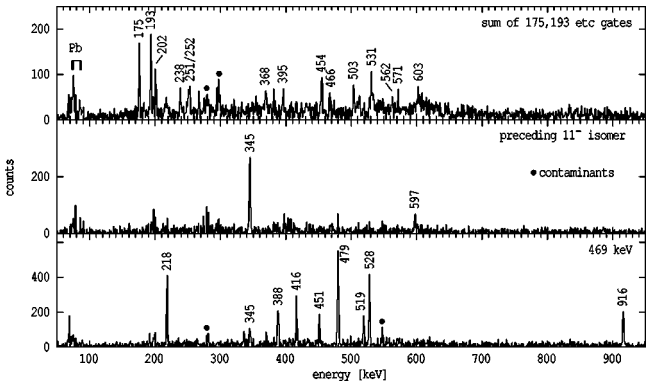

FIG. 5. Top panel: Sum of individual gates above the 8^- isomer, with additional gates on delayed transitions. Middle panel: Spectrum of transitions gated on delayed transitions within the 11^- band. Bottom panel: Prompt coincidences with the 469 keV transition, with additional gates on delayed transitions that follow the 11^- isomer.

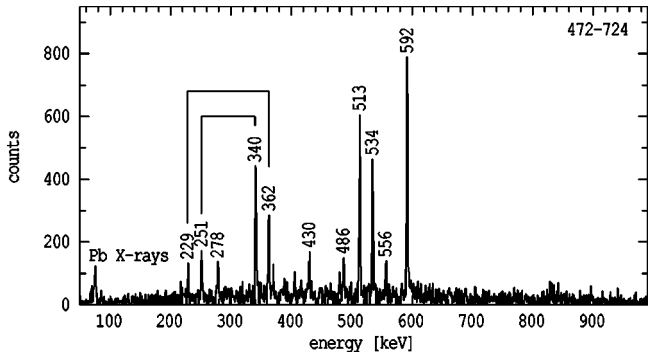

FIG. 6. Triple coincidence spectrum with gates on the 472 and 724 keV transitions in ^{188}Pb, selecting transitions connecting the yrare and yrast positive parity bands, as discussed in the text.

the total conversion coefficient for the 218 keV transition is not precisely defined but it is sufficient to exclude $M1$ multipolarity and high-order multipolarities, leaving only $E1$ or $E2$ alternatives, and therefore spin and parity of 18^+ or 19^- for the 4783 keV state. The conversion favors the $E2$ possibility and the angular distribution for the 218 keV transition is suggestive of a stretched quadrupole, but the error is large. Given the possibility of attenuation from the long lifetime and the presence of contaminant 218 keV transitions, only a tentative assignment of 19^- has been made.

Note that the 566.6 branch connecting the 15^- 4096 keV state to the 14^+ yrast state and the various connections from the 3680 keV 13^- state to states in the (5^-) band shown on the extreme right of Fig. 1, which themselves have branches to a range of yrast states, results in a path which bypasses the 38 ns, 11^- state and results in a long feeding component to the yrast band, in addition to that caused by the 8^- isomer.

Considering the states above the 12^+ isomer, the stretched quadrupole nature of the 990 keV transition suggests 14^+ for the 3700 keV state which also has a branch to the 12^+ 2924 keV state. The 4512 keV state decays to the 14^+ yrast sequence and has branches of 813 keV to the 14^+ 3700 keV state and a 268 keV transition with a large negative A_2/A_0 coefficient to the 4245 keV state. That state has a 545 keV (likely dipole) transition to the 14^+ state at 3700 keV and another branch (undefined distribution) to the 14^+ state at 3530 keV. Consideration of these branches leads to the 15^+ and 16^+ suggestions for the 4245 and 4512 keV states, respectively.

2. Non-yrast states and E0 transitions

A key element in the assignments for the low spin states is the observation of $E0$ components in the transitions connecting the yrare states to the yrast band (Fig. 2). The evidence for these is contained in coincidence spectra such as that obtained by gating on both the 471.5 keV $6^{+\prime}$ to $4^{+\prime}$ in-band transition and the 724 keV 2^+ to 0^+ transition shown in Fig. 6.

The requirements that the 251 keV transition must balance the 340 keV, $4^+ \rightarrow 2^+$ $E2$ transition, and similarly, that the 229 keV connecting transition must balance the 362 keV in-band transition, can only be satisfied if both connecting transitions have large total conversion coefficients. These total conversion coefficients were compared with theoretical values for $E1$, $M1$, and $E2$ multpolarities in Table I. In the absence of significant lifetimes for the initial states, only $E1$, $M1$, or $E2$ γ-ray multipolarities need to be considered. At these energies, the hierarchy of total conversion is $\alpha_T(M1) > \alpha_T(E2) > \alpha_T(E1)$, and since the observed values exceed the $M1$ value, a significant $E0$ conversion component is implied. This is the case for each of the connecting transitions observed, resulting in the J^π to J^π assignments, to be discussed further below.

When both bands have $K=0$, a further simplication is possible since the relevant Clebsch-Gordan coefficient for $J \rightarrow J$ $M1$ transitions, vanishes. The observed total conversion $\alpha_T(\exp.)$ and the theoretical value for $E2$ multipolarity is then related to the $E2$ and $E0$ decay widths for the J to J transition simply by

$$\alpha_T(\exp.) = \alpha_T(E2) + \Gamma_e(E0)/\Gamma_\gamma(E2),$$

allowing the extraction of width ratios for the $J \rightarrow J$ transitions.

3. 8^- isomer at 2577.1 keV

The present coincidence results have confirmed the 103, 710, and 360 keV branches from the isomer proposed previously [10], and clarified the states and transitions in the subsequent decay path. Similarly, the 278 keV branch from the isomer has been firmly established, and its specific connecting paths beginning at the 2299 keV state, delineated. A new branch of 129 keV has also been established. The difficulty in resolving these paths in the previous work was exacerbated by a number of close doublets, which we have now identified and unambiguously placed, using double gating. These include the 360.2 and 362.4 keV transitions, the 429.2 and 430.6 keV transitions, and the 471.5 and 472.9 keV transitions. These transitions are seen in the double-gated spectra (Fig. 7) produced from the γ-γ-γ cube, restricted to the out-

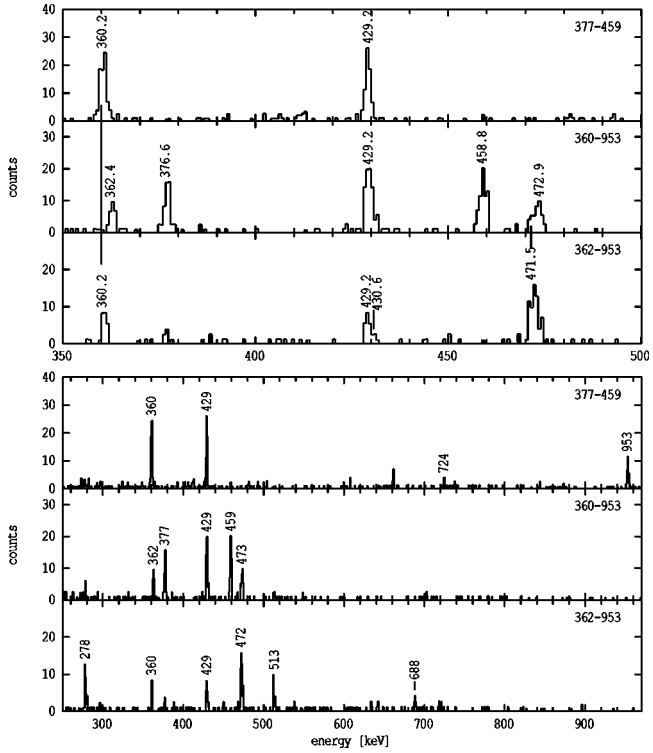

FIG. 7. Double-gated spectra for transitions below the 8^- isomer. The upper part of the figure shows the spectra expanded over the region where several doublets occur.

of-beam region. An expanded version is shown in the upper part of Fig. 7.

The transition strengths deduced from the measured branching ratios are listed in Table III. The strengths are given in terms of the hindrance factor $F=\tau/\tau_W$, the ratio of the partial mean lives to the Weisskopf estimates τ_W, and the reduced hindrances $f_\nu=F^{1/\nu}$, where the degree of forbiddenness for multipolarity λ is given by $\nu=\Delta K$-λ. With the present assignments, most f_ν values fall within the range of ~20–100 expected for deformed configurations where K is conserved. The main exception is the 103 keV transition which would favour a $K=3$ alternative for the 7^- state.

The states below the isomer will be discussed later but it is relevant for the assignment of the isomer, that the 2299 keV state is firmly assigned as 8^+, while the 278 keV connection to the isomer has $\alpha_T=0.08(5)$ which is consistent with $E1$ multipolarity or, at the extreme, $E2$ multipolarity, but not $M2$. As partly argued previously [10], a direct connection to the 8^+ yrast state and the absence of a direct decay from the isomer to the 6^+ yrast state confined the likely spins and parities of the isomer to be 8^-, 9^+, or 9^-, of which only the 8^- and 9^- possibilities would satisfy the restriction on the 278 keV transition. As will be discussed below, the main decay from the isomer is a 360.2 keV transition to the 2474.0 keV (7^+) state. Intensity balances give a conversion coefficient limit which is only compatible with $E1$ multipolarity, hence the 9^- possibility can be eliminated, leading to a firm assignment of spin and parity 8^-.

Transitions directly feeding the 8^- isomer are shown in the top panel of Fig. 5. Population in this band drops off quickly with spin and the band is perturbed by an interaction between two 11^- states. The angular distributions for the 175 and 193 keV transitions and several other cascade transitions have large negative A_2/A_0 coefficients, consistent again with mixed $M1/E2$ multipolarities.

B. Yrare states and associated non-yrast structures

1. States at 2448.4 and 2474.0 keV and their decays

The conversion coefficient of the weak 129 keV branch from the 8^- isomer to the 2448.4 keV is relatively large [2.0(13), Table I] suggesting $E2$ multipolarity and therefore a spin and parity of 6^- for the 2448.4 keV state. No additional spectroscopic information is available for transitions feeding that state but the branches are consistent with the sequence 6^-, 8^-, 10^- as shown.

The 103 keV transition from the 8^- isomer to the 2474.0 keV state has a probable $M1$ assignment from the measured total conversion (Table I) suggesting spin and parity 7^- for that state, supported by branches to the 6^+ and 8^+ yrast states. Both of these transitions, however, are contaminated and reliable angular distributions were not available. Nevertheless, the quadrupole character of the 518 keV branch to the 1995.9 keV state, which itself decays by the 892.4 keV transition of stretched dipole character (Table II), and hence has a probable 5^- assignment, supports the 7^- assignment for the upper state. The angular distribution for

TABLE III. Branching ratios and transition strengths for decays from the 2577 keV, 8^- and 4783 keV (19^-) isomers in ^{188}Pb.

Final State J^π	E_γ (keV)	I_γ relative	$M\lambda$	α_T	$B(E\lambda)$ (e^2 fm$^{2\lambda}$)	Trans. Strength (W.u.)	ν	f_ν
8^-, 2577 keV	1150(30)ns							
7^-	103	20(3)	$M1$	9.12	$1.63(27)\times10^{-6}$	$9.1(1.5)\times10^{-7}$	(6,4)	(10.2, 32)[a]
(6^-)	129	21.3(25)	$E2$	2.24	$7.61(10)\times10^{-1}$	$1.19(16)\times10^{-2}$	(1)	(84)
8_1^+	278	69.6(30)	$E1$	0.036	$3.18(24)\times10^{-10}$	$1.50(12)\times10^{-9}$	7	18.2
7^+	360	148(5)	$E1$	0.020	$3.12(22)\times10^{-9}$	$1.47(11)\times10^{-9}$	5	58
8^+	710	61(3)	$E1$	0.005	$1.68(13)\times10^{-10}$	$7.9(6)\times10^{-11}$	7	27.8
(19^-), 4783 keV	630(80)ns							
17^-	218	100	$(E2)$	0.323	2.0(3)	$3.1(4)\times10^{-2}$	(6)	(1.8)

[a]The two alternatives correspond to the assumption of either $K=1$ or $K=3$ for the 7^- state.

the 793.1 keV transition from the 1516.6 keV state is also consistent with a stretched dipole although the remaining intensity at this level is low, and hence the error is large. The 1219 keV state at the bottom of this sequence (see Fig. 2) could be a 1^- member, but there is no spectroscopic information on the (very weak) 298.2 and 1219 keV transitions.

The other two main sequences in this spin region exhibit complex decays to both the yrast sequence, and to what we have assigned as the yrare positive-parity sequence. As stated earlier, a key factor in this assignment is the observation of larger than expected total conversion coefficients for the 228.7, 250.8, and 352.6 keV transitions connecting the 952.5, 1314.9, and 1786.4 keV states to the 2^+, 4^+, and 6^+ states of the yrast band. The presence of $E0$ components deduced from these results, listed in Table I, is only possible if there is no change of spin or parity. From Table II, the 228.7 and 250.8 connecting transitions have significant negative A_2/A_0 coefficients, which would indicate either stretched dipole transitions ($\Delta J=\pm 1$) or $\Delta J=0$ transitions with large quadrupole admixtures of 50–100%. The latter alternative might seem unusual but as argued earlier, $J\rightarrow J$ transitions between $K=0$ bands would have no $M1$ component, leaving at the extreme, only a quadrupole ($E2$) γ-ray component, in agreement with the present assignment. The assignments are consistent with the distribution for the 591.5 keV transition, which has a positive A_2/A_0 coefficient, although this by itself would not be sufficient for the 4^+ assignment to the 1314.9 keV state because of the ambiguity between $\Delta J=0$ and $\Delta J=2$ distributions. All other spectroscopic information we have, including branches to other states, and for example, the conversion coefficient for the 278 keV transition connecting the 8^- isomer to the 2299.4 keV state discussed earlier, support these assignments, as does the population of the states. (Further comment is provided in the next subsection.)

The limit on the conversion coefficient of the strong 360.2 keV branch from the 8^- isomer to the 2217.1 keV state suggests $E1$ multipolarity, while the 783.7 branch from that state to the 6^+ yrast state has a very large, positive A_2/A_0 value and therefore is probably of mixed $M1/E2$ character, both observations supporting a 7^+ assignment to the 2217.1 keV state. A reliable independent distribution for the 429.2 keV transition to the 1787.9 keV state was not obtained because of the proximity to the competing 430.2 keV branch to the 1786.4 keV (6^+) state. Since the 724 keV branch from the 1787.9 keV state to the 4^+ yrast state coincides in energy with the 2^+ to 0^+ transition, its distribution is also not obtained. The 376.6 keV branch to the 1411.3 keV state, however, has a very large positive A_2/A_0 value (similar to that of the 783.7 keV transition discussed above), which could be interpreted as a mixed $M1/E2$ $5^+\rightarrow 4^+$ transition.

These assignments result in different spins for the doublet of states at 1786.4 and 1787.9 keV, whose close spacing would be difficult to understand if they had the same spin and parity. It also leads to consistent branches to and from other states. For example, the 2474.0 keV, 7^- state has an $E1$ branch to the 1786.4 keV, 6^+ state but not an $M2$ branch to the 1787.9, 5^+ state.

2. Alternative assignments from other work

We are aware of contemporary studies of ^{188}Pb that imply conflicting assignments for some states and specific decay properties which may also be in conflict with the present scheme. While these studies have yet to be reported in full, it is appropriate to focus on some of the current experimental results which may bear on those assignments.

Recent electron experiments involving the observation of electrons in coincidence with delayed recoils [24] observed strong transitions at 591 and 724 keV, which at the time were suggested to be associated with the decay of 0^+ states in ^{188}Pb, although the lines observed are not necessarily in ^{188}Pb. Since the preliminary reporting of the present results, in which 591 and 723 keV γ-ray connections between the yrare and yrast states have been observed, the possibility has been raised that the electrons observed by Le Coz *et al.* [24] should be associated with those transitions. In turn, because of the electron intensity, this would imply $E0$ components and therefore spin assignments which are two units lower than those deduced in the present work.

From the preceding discussions and the other experimental properties reported here, however, there is little scope within our results for such alternative assignments. (Note that the population of the yrare states is relatively low and $E0$ conversion electron lines from the 353 keV transition identified here, for example, would have been below the sensitivity of the electron experiments of Ref. [24].)

3. Branches to excited 0^+ states

The situation with the excited 0^+ states is that the weighted mean of reported results for the $0^{+\prime}$ state [18,24–27] is 573(3) but individual values vary from 568 to 591 keV. A very recent measurement by Van de Vel *et al.* [28] of the α decay of ^{192}Po gives an energy of 588(4) keV which compares with the 568(4) keV given by Allat *et al.* [18], values which are inconsistent within the quoted errors.

The two values reported for the $0^{+\prime\prime}$ state of 767(12) keV (α decay [18]) and 725(2) keV (in-beam conversion electrons [24]) are essentially incompatible and neither has been confirmed in the most recent α-decay studies [28], hence the position (and indeed existence) of a $0^{+\prime\prime}$ state remains uncertain.

Given the uncertainties, the possibility of identifying excited 0^+ states via γ-ray branches from the 2^+ states which in principal are members of the same bands, takes on an importance in addition to the testing of the proposed band structures in terms of predicted branching ratios. This is experimentally difficult because the transitions in absolute strength are expected to be weak. They must compete with much higher energy branches to the ground state and, of course, there is no subsequent γ decay.

We have searched for such branches, particularly in the delayed γ-γ-γ cube where double gates can be set on pairs of transitions that feed the 953 keV, $2^{+\prime}$ state, for example, where contaminant transitions are minimal. The most likely branch is to the $0^{+\prime}$ state, which (given the uncertainty in state energy outline above) should result in a transition in the range 360–389 keV. The γ ray would have to be common to pairs of double gates on transitions feeding the 953 keV state in the delayed region. No unassigned transitions that satisfied these criteria were identified. There remains the possibility that such a transition coincides in energy with either the 360

TABLE IV. Branching ratios and $(g_K - g_R)/Q_0$ values for states associated with bands in ^{188}Pb.

J^π	$E_\gamma(\Delta J=1)$ (keV)	$E_\gamma(\Delta J=2)$ (keV)	λ[a]	$\lvert g_K\text{-}g_R\rvert$[b] Exp.	Theory[c]
$K^\pi=8^-$	2577 keV				$-0.30(1)$
13^-	250.5	503.0	1.47(51)	0.304^{+83}_{-49}	
12^-	252.2	454.1	2.65(77)	0.115^{+44}_{-34}	
$11^{-\prime}$	238.2	431.2	1.15(29)	0.173^{+41}_{-30}	
11^-	201.6	394.9	0.86(21)	0.233^{+44}_{-30}	
10^-	193.0	368.1	0.68(26)	0.161^{+63}_{-39}	
$K^\pi=11^-$	2702 keV				$+0.74; +0.63$[d]
$13^{-\prime}$	451.0	978.6	0.68(7)	0.27(2)	
13^-	387.7	915.5	1.33(8)	0.195(9)	

[a]λ is the ratio of crossover/cascade γ-ray intensities.
[b]Taking $Q_0=6.5$ and 5.0 eb for the 8^- and 11^- bands, respectively.
[c]Assuming $g_R=+0.30$.
[d]The smaller value corresponds to the use of an empirical value of $g_K=+0.51$ for the $9/2^-[505]$ proton orbital.

or 362 keV transitions that are placed in the decay path of the isomer and feed the 953 keV state. This possibility was also tested by double gating on the 362 and 513 keV transitions, thus eliminating coincidences with the 360 keV decay from the 8^- isomer which is in a parallel path. No significant intensity was observed near 362 keV, hence this possibility can be eliminated, at least at the level of the present statistics.

C. Band properties

Table IV lists the in-band branching ratios for transitions in the 8^- and 11^- bands, from which the values of $g_K - g_R$ have been extracted, using the standard rotational model formulae.

Also listed in the table are theoretical values for the proposed configurations, to be discussed later.

VI. STRUCTURE ANALYSIS AND PHENOMENOLOGICAL APPROACHES

In order to put the experimental results into context, two approaches were taken, an analysis of the low-spin sequences in terms of band mixing, and multiquasiparticle calculations to predict the lowest-lying two and four quasiparticle high-K states expected from prolate and oblate deformations.

A. Three-band mixing

State-mixing calculations for this region have been reported before, and they range from two-band explorations of the properties of the yrast sequence carried out in the context of shape coexistence in Pt, Hg, and Pb isotopes [29] to more specific two-state mixing [17,30–32] and three-state mixing [18] focused on the low-lying 0^+ states and their population through α decay. The last obviously depends on configuration mixing in both the parent (Po) isotope and the states of the Pb daughter.

With the new results on non-yrast states identified in the present work, more constrained analyses are now possible. With that in mind, the present band-mixing calculations were aimed initially at reproducing the energies of both yrast and non-yrast sequences. The formalism used is similar to that reported before [29] and is now commonly used in this region. The initial inputs to the calculations are the energies of three unperturbed sequences. For the oblate and prolate sequences it is natural to parametrize these with the variable-moment-of-inertia (VMI) formalism which is convenient for describing bands which are weakly- or well-deformed.

It is less obvious how the notionally spherical sequence should be treated. The simplest approach is to again use the VMI form with a very low moment of inertia. If mixing only occurs with say, the 2^+ states, the others being significantly non-yrast, this would be a reasonable approximation. Calculation of the even-spin positive-parity states within the shell model is not practical in the middle of the neutron shell. The availability of a large number of neutron-hole orbitals leads to mixed configurations derived from the sequences expected for two particles in a j^2 multiplet whose energy spectrum can, in principal, be used as a guide to represent the spherical states. A more pragmatic approach is to approximate the unperturbed spectrum by extrapolating from the (predominantly) spherical sequences known in ^{190}Pb, ^{192}Pb, and the heavier isotopes, and to model that sequence with a convenient functional form. Each of these approaches has been explored.

For simplicity, spin-independent interactions have been used, noting that any monotonic spin-dependence in the interactions can usually be compensated for by a corresponding adjustment to the unperturbed moments of inertia, leading to an inherent ambiguity, particularly when the spin range over which the fits are carried out is small. (Further comment on the magnitude of the interactions is made below.)

The newly observed non-yrast states, and the excited 0^+ states can be included in the fits. Compared to previous

band-mixing analyses, these mixing calculations are much more constrained because of the experimental states now identified. However, there is still considerable leeway because the third 2^+ state has not been observed, a possible third 4^+ state (1411 keV) is placed but the spin/parity assignment is tentative, and the energies of the excited 0^+ states have been disputed as discussed earlier, hence a range of values has to be considered in choosing the fits.

The fits yield moment-of-inertia parameters for the unperturbed bands, limits on the interaction matrix elements, and the values of the mixing amplitudes. The unperturbed moment-of-inertia parameters can be related to the deformation and therefore quadrupole moment of the unperturbed bands through the VMI equivalent of the Grodzin's formula. The approach taken here is to use these moments, together with the calculated amplitudes, to calculate the $B(E2)$ and $B(E0)$ transitions using the general formulation given by Kibédi *et al.* [33]. The corresponding decay widths which are, in essence, predictions, can be compared with widths and branching ratios extracted from experiment.

1. Other band-mixing models

A less-specific, theoretically oriented band-mixing approach taken recently by Fossion *et al.* [34] describes the assumed three components within the IBM model, taking the configurations as notional $0p$-$0h$, $2p$-$2h$ and $4p$-$4h$ excitations. The parameters are adjusted to experimental levels in Pb, Pt, and W nuclei and the mixing matrix elements are partly constrained by the model description, thus reducing the otherwise large number of parameters. Those calculations, however, are not expected to give detailed agreement with experiment without further fitting (to the new results given here, for example) and therefore cannot be tested quantitatively. One simplification in their model is that only mixing involving two-particle excitations is allowed, hence there is no direct matrix element between the $0p$-$0h$ excitations (notionally the spherical configuration) and the $4p$-$4h$ excitations (notionally the prolate deformed configurations) and there is an approximate relationship that the mixing matrix element between the $0p$-$0h$ and $2p$-$2h$ configurations is about half the magnitude of that between the $2p$-$2h$ and $4p$-$4h$ excitations. Bengtsson and Nazarewicz [7] also suggest from their configuration-constrained mean-field approach that interaction matrix elements between configurations involving different numbers of intruder orbitals are likely to be small, although they do not give a quantitative estimate.

In the present calculations, we have also explored the results obtained if the equivalent spherical-prolate matrix element is taken as zero.

2. Transition strengths

In calculating quantities related to the transition strengths, explicit use is made of the mixed amplitudes and the intrinsic properties of the unperturbed bands. In general then, as in Ref. [33] we write the electric transitions as

$$B(EL;J_i \rightarrow J_f) = \left[\sum_{jk} A_k^i A_l^f \langle k|\mathbf{EL}|l\rangle \right]^2, \tag{1}$$

where $k,l\ldots$,etc., label the unperturbed bands and the A_k^i and A_l^f are the amplitudes from the band-mixing calculations. For rotors of quadrupole deformation

$$\beta_k = \frac{\sqrt{5\pi} Q_o(kk)}{3ZR_o^2}, \tag{2}$$

and $E2$ transitions from the "diagonal" terms in the summation above connecting components of the same intrinsic configuration are given by

$$\langle k|\mathbf{E2}|k\rangle = \sqrt{5/16\pi}\,\langle J_i 2K0|J_f K\rangle e Q_o(kk). \tag{3}$$

The off-diagonal terms (connecting components of different intrinsic configuration) can be taken as zero or commonly and somewhat arbitrarily, as a proportion of the average diagonal terms, for example,

$$Q_o(kl, k \neq l) \sim \frac{1}{8}\left[\frac{Q_o(kk) + Q_o(ll)}{2} \right]. \tag{4}$$

The same mixed amplitudes are involved in the calculation of $E0$ strengths with "diagonal" matrix elements given by

$$\langle k|\mathbf{E0}|k\rangle = (3Ze/4\pi)R_o^2\beta_k^2 = \frac{5eQ_o^2(kk)}{12ZR_o^2}. \tag{5}$$

Correct treatment of the intrinsic off-diagonal term ($k \neq l$) is only possible with a microscopic description of the wave function in deformation space, as has been emphasized before [35]. It would lead in the case of transitions between a vibrational state built on an equilibrium deformation (of magnitude β_k), and the nonvibrational state, to a matrix element of the form

$$\langle k|\mathbf{E0}|l\rangle = (3Ze/4\pi)R_o^2\beta_k\langle k|\beta - \beta_k|l\rangle, \tag{6}$$

proper treatment of which would require an evaluation of the fluctuation in deformation.

Transitions within the unperturbed spherical multiplet are approximated by a j^2 configuration with

$$B(E2) = e_{eff.}^2\langle r^2\rangle^2 \times (2J_f+1)\begin{Bmatrix} j & J_f & j \\ J_i & j & 2 \end{Bmatrix}^2 \times (2j+1)^2\left\langle j2j|-\frac{1}{2},0,\frac{1}{2}\right\rangle^2 \tag{7}$$

with an effective charge $e_{eff.}=0.5$ and mean-square charge radius $\langle r^2\rangle = 44$ fm^2. Although the choice of orbital spin j determines the spin dependence within the multiplet, the magnitude of the $B(E2;2\rightarrow 0)$ values, which are the main ones of importance here since the mixing is predominantly at low spin, are nearly independent of the assumed value of j. For comparison it should be noted that a typical value for such a $2\rightarrow 0$ transition corresponds in magnitude to a rotational transition for an intrinsic quadrupole moment of $\sim 0.5\ e$b.

3. Interference in two-band mixing

Before proceeding, it may be useful to examine the effects of interference for $E2$ and $E0$ $J \rightarrow J$ transitions implied in Eq. (1) above. In the case of two-band mixing, the amplitudes are such that

$$|i\rangle = a|k\rangle + b|l\rangle,$$

$$|f\rangle = -b|k\rangle + a|l\rangle,$$

$$\text{with } a^2 + b^2 = 1.0.$$

Hence, from Eq. (1)

$$\sqrt{B(EL)} = ab(\langle l|\mathbf{EL}|l\rangle - \langle k|\mathbf{EL}|k\rangle) - (b^2 - a^2)\langle k|\mathbf{EL}|l\rangle. \tag{8}$$

The first term depends on the difference in deformation (or quadrupole moment as given earlier) and is a maximum, for a given deformation difference, at complete mixing. The second term vanishes at complete mixing, and depending on the magnitude of the intrinsic matrix elements, may be significant when the first term is small, which can be the case for small differences in deformation. As argued recently [36] in considering $E0$ transitions, if the deformations are sufficiently well separated (in configuration space) it may be possible to neglect the second term. In that case, in terms of a deformation β, we have

$$\sqrt{B(E2, J \rightarrow J)} \sim ab[\beta_1 - \beta_2],$$

with the corresponding relationship for $E0$ transitions being

$$\rho(E0, J \rightarrow J) \sim ab[(\beta_1)^2 - (\beta_2)^2],$$

where $\rho = B(E0)/R_0^2$.

Both strengths, which are directly related to the decay widths $\Gamma(E0)$ and $\Gamma(E2)$ are only nonzero if a is neither zero nor unity, and if the deformations, β_1 and β_2 are not equal as has been emphasized several times (see for example Refs. [35–37]). The importance of the $E0$ components is therefore not just that they restrict the spin and parity assignment, but that such $E0$ and $E2$ widths are likely to arise only if there is significant mixing and deformation difference.

B. Mean-field calculations and multiquasiparticle states

To predict the spectrum of high-K multiquasiparticle states that can be expected, calculations have been carried out using deformation parameters similar to those of the coexisting minima given by various mean-field approaches. Calculation of the expected multiquasiparticle-state spectrum used the approach outlined in recent publications (see, for example, Ref. [38]) with the modification that a Lipkin-Nogami treatment of pairing is used, rather than BCS. The procedure involves first, a choice of single-particle levels and the pairing strength. The calculations use the prescription given by Nazarewicz *et al.* [39] to treat the Fermi level and pairing gaps self-consistently, to include particle-number conservation, and to have blocked states removed for multiquasiparticle configurations.

For the present calculations, a space of three oscillator shells giving 64 levels (128 states) with 42 protons and 66 neutrons active was used, taken from the Nilsson scheme with deformations of $\epsilon_2 = -0.16$ (oblate) and $\epsilon_2 = 0.236$ (prolate). Pairing strengths were given by $G_\pi = 22.1$ MeV/nucleon and $G_\nu = 17.1$ MeV/nucleon.

The excitation energies so calculated will be relative to the base of the oblate and prolate submimima in the potential well. These were taken arbitrarily as 600 keV for the oblate minimum and 750 keV for the prolate minimum as indicated in Table V. Alternatively, if specific states can be characterized, their excitation could provide an estimate of the combined pairing gap and energy of the minima.

A more sophisticated approach is provided by calculations within the configuration-constrained potential energy surface framework developed by Nazarewicz, Wyss, Xu, and coworkers, in which the deformation is calculated self-consistently for a given configuration. That model [42] using a Woods-Saxon potential, was applied to calculation of the $K^\pi = 8^-$ two-quasineutron prolate isomer in ^{188}Pb [41] and to the $K^\pi = 11^-$ two-quasiproton oblate isomer in ^{188}Pb [40], the latter of which included quadrupole pairing. The calculations gave energies of 2400 keV for the 8^- configuration with a prolate deformation of $\beta_2 = 0.26$, and 2726 keV for the 11^- state with an oblate deformation of magnitude $|\beta_2| = 0.19$. Xu notes [40] that the 11^- isomer is not soft in shape, unlike the potential energy surfaces for the coexisting 0^+ states and, to some extent, the 8^- prolate state.

VII. DISCUSSION

The expectation [12] that different *isomeric* states with certain spins and parities would arise from two-particle excitations at each of the predicted deformations guided the earlier work which subsequently identified four isomers in ^{188}Pb, three of which were firmly placed [10]. (As stated in the introduction, the prompt yrast sequence in ^{188}Pb was in fact the first band in the neutron-deficient Pb isotopes associated with a low prolate well [1] mainly on the basis of the superficial character of the band—its regularity above spin 4^+ and the similarity of its moment of inertia to those of bands in the neutron-deficient mercury isotopes.) The three lowest isomers were associated [10] with a 12^+ state from the $i_{13/2}^{-2}$ neutron-hole configuration characteristic of *sphericity*; a $K^\pi = 11^-$ intrinsic state from the excitation of two protons into the $\Omega = j$ Nilsson orbitals, $9/2^-[505]$ and $13/2^+[606]$, which are near the Fermi surface at *oblate* deformation; and a two-quasineutron state with $K^\pi = 8^-$, from the $9/2^+[624] \otimes 7/2^-[514]$ configuration which is the lowest two-quasiparticle high-K isomer in *prolate* nuclei with $N = 106$. These interpretations are now largely confirmed through the identification of the structures above the isomers.

To provide an overview, the observed states in ^{188}Pb are shown in Fig. 8, which gives the excitation energies relative to those expected for a well deformed rotor with an arbitrary moment of inertia. Where appropriate, states are grouped into band structures.

TABLE V. Calculated high-K deformed configurations for ^{188}Pb.

K^π	Shape[a]	Configuration[b]		E_{calc}[c] (keV)	$E_{exp.}$ (keV)	g_K-g_R[d]	sign[δ]	Ref.[e]
		ν	π					
11^-	o	…	$9/2^-\ 13/2^+$	2640	2702	+0.74	−ve	
	o	…	$9/2^-\ 13/2^+$	2726				[40]
8^+	o	$7/2^+\ 9/2^+$	…	2002		−0.48	+ve	
7^-	p	$7/2^+\ 7/2^-$	…	2214		−0.61	−ve	
8^-	p	$7/2^-\ 9/2^+$	…	2151	2577	−0.31	−ve	
		$7/2^-\ 9/2^+$	…	2400				[41]
7^+	p	$7/2^-\ 7/2^{-'}$	…	2398		−0.35	−ve	
8^+	p	$7/2^+\ 9/2^+$	…	2331		−0.55	−ve	
15^+	p	$7/2^-\ 9/2^+\ 7/2^+ 7/2^{-'}$	…	4167		−0.19	−ve	
19^-	o	$7/2^+\ 9/2^+$	$9/2^-\ 13/2^+$	4035	4783	+0.23	−ve	

[a] o: oblate; p: prolate.
[b] Prolate configurations: (π) $9/2^-$: $9/2^-[514]$; $7/2^+$: $7/2^+[404]$; $7/2^-$: $7/2^-[523]$: (ν) $11/2^-$: $11/2^-[505]$; $9/2^+$: $9/2^+[624]$; $7/2^+$: $7/2^+[633]$; $7/2^-$; $7/2^-[514]$; $7/2^{-'}$; $7/2^-[503]$; oblate configurations: (π) $9/2^-$: $9/2^-[505]$; $13/2^+$: $13/2^+[606]$; (ν) $11/2^+$: $11/2^+[615]$; $9/2^+$: $9/2^+[624]$; $7/2^+$: $7/2^+[633]$; $3/2^-$: $3/2^-[512]$; $5/2^-$: $5/2^-[503]$.
[c] Energies from the present calculations assume that the oblate minimum is at 600 keV and prolate minimum is at 750 keV.
[d] Taking $g_R = 0.30$.
[e] This work unless otherwise stated.

A. Two- and four-quasiparticle configurations

1. $K^\pi = 11^-$ isomer at 2702 keV; oblate configuration

The states above the 11^- isomer correspond to structures which are similar to those observed in ^{190}Pb and ^{192}Pb [9,43], however the states do not form a simple, single rotational band. $\Delta J = 1$ transitions are observed between the first few states, followed by a $\Delta J = 2$ sequence. The sequence is perturbed by a second 13^- state, arising, as is apparent from an inspection of Fig. 8, from a crossing with a $\Delta J = 2$ sequence with high alignment beginning at the 2210.3 keV 5^- state shown on the right of Fig. 1. (It is possible that one or the other of the 4250.0 and 4408.9 keV states is associated with these bands.) If the 3617 and 3680 keV 13^- states are assumed to be maximally mixed, the unperturbed states would have originated at about 3649 keV.

The similarity of the lower part of the sequences in ^{188}Pb, ^{190}Pb, and ^{192}Pb can be seen from Fig. 9, where the three cases are compared to the one-quasiproton bands in ^{187}Tl from the two Nilsson orbitals, $9/2^-[505]$ and $13/2^+[606]$ [44], the proposed constituents of the 11^- configuration. While the sequences are limited in extent, the bands are similar in slope, and they have similar levels of perturbation, supporting the proposed configuration. The steep slope in

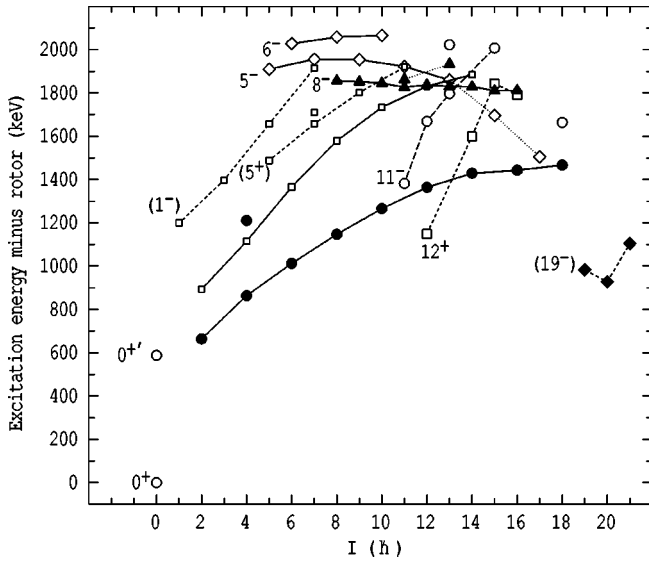

FIG. 8. Energies of excited states in ^{188}Pb plotted relative to an arbitrary rigid rotor (with $E = 10 \times I(I+1)$ keV).

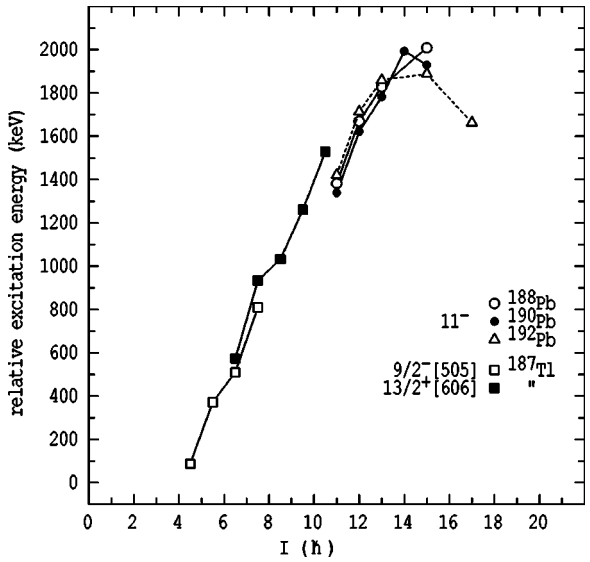

FIG. 9. Energies of one-quasiproton bands in ^{187}Tl plotted relative to an arbitrary rigid rotor [with $E = 10 \times I(I+1)$ keV] compared to the 11^- bands in ^{188}Pb, ^{190}Pb, and ^{192}Pb.

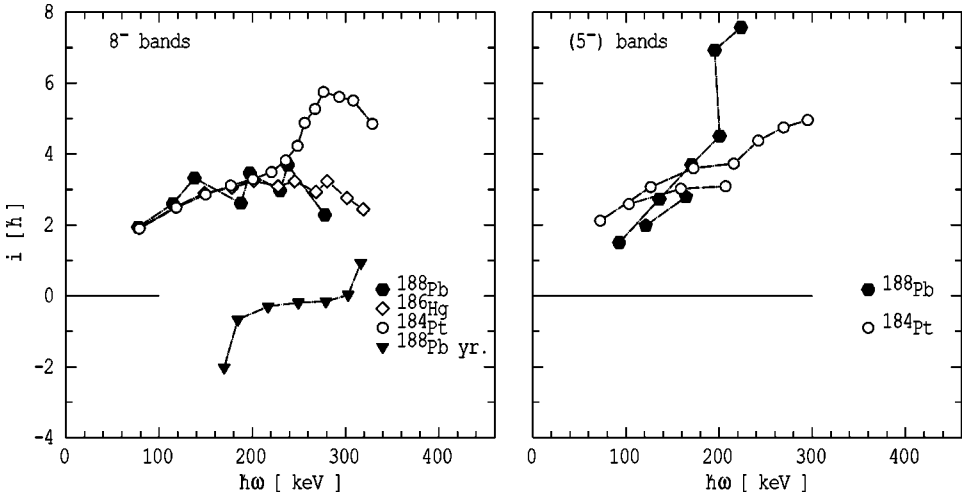

FIG. 10. Alignments of the sequences above the 8^- isomer in ^{188}Pb compared to 8^- bands in the $N=106$ isotones and the yrast band (left panel); alignment of the 5^- sequence in ^{188}Pb compared to that of the known band in ^{184}Pt (right panel). Reference parameters are $\Im_0=27$ MeV$^{-1}\hbar^2$ and $\Im_1=190$ MeV$^{-3}\hbar^4$.

this plot however, is indicative of a deformation which is small compared to that of the 8^- prolate band, for example. Its equivalent curve on this scale is essentially flat, as seen in Fig. 8.

The crossover/cascade γ-ray branching ratios (λ) have been used to extract g_K-g_R values, as shown in Table IV. (The assumed value of $Q_0=-5.0$ eb is about the maximum value consistent with the proposed deformation.) The only values available are from the branching of the two 13^- states at 3617 and 3680 keV, and these are of similar magnitude, consistent with the argument given above that the states are substantially mixed.

The cascade transitions have large negative A_2/A_0 coefficients, implying a negative sign (δ) and, therefore, for a negative quadrupole moment, a positive sign for g_K-g_R. This gives $g_K-g_R\sim+0.2$ which is significantly smaller than the theoretical value (obtained with $g_R=+0.30$) of $g_K-g_R\sim+0.7$. In effect, the pure two-proton configuration would predict much weaker crossover transitions than are observed. It seems that the band properties (approximate moments of inertia, for example) agree with the proposed assignments but the detailed band properties are not consistent with rotation of a simple oblate deformation.

Taken at face value, the perturbations in the bands (11^- and one-quasiproton) also imply mixing effects which are not consistent with pure K, despite the fact that the proton Fermi surface is close to the $\Omega=j$ orbital for both proton components. A simplified calculation involving coupling of the set of $i_{13/2}$ Nilsson orbitals to the $9/2^-[505]$ orbital, including Coriolis matrix elements has been carried out to estimate the magnitude of K mixing expected. For the 11^- band significant components of $K=10$ and $K=9$ admixtures are found. However, when these are included explicitly in the extraction of g_K-values from the branching ratios, which is strongly K, dependent, the extracted value is still only marginally larger than if pure $K=11$ is assumed, hence this does not resolve the problem. As well, while the average moment of inertia is reproduced, the band is expected to be regular, whereas clearly it is not. Such discrepancies might be attributable to γ-asymmetric distortions, however, the configuration-constrained potential-energy-surface calculations of Xu [40] for the $13/2^+[606]\otimes 9/2^-[505], 11^-$ configuration predict a well-defined symmetric oblate deformation, without significant γ softness. A similar result was obtained recently by Smirnova *et al.* using the self-consistent Hartree-Fock-Bogoliubov method with a Skyrme interaction [45]. (Neither of these calculations, however, include the dynamic effects of rotation.)

2. $K^\pi=(19^-)$ isomer at 4783 keV

Although its spin and parity are not precisely defined, this state is an obvious candidate for the 19^- state predicted at 4035 keV in the multi-quasiparticle calculations (Table V). Its configuration involves coupling of the 11^- two-proton excitation to the 8^+ two-neutron excitation at oblate deformation. The energy is underestimated but that will depend to some extent on assumed deformation. Note that because the neutron Fermi surface is near the middle of the $i_{13/2}$ neutron shell, equivalent 8^+ configurations arise from the $7/2^+[633]\otimes 9/2^+[624]$ configuration at both prolate and oblate deformations. The 8^+ configuration will also have significant Coriolis mixing which together with the proposed mixing in the 11^- configuration, might be responsible for the low hindrance observed for the 218 keV transition. It has a nominal forbiddenness of $\nu=6$, but the transition strength is orders of magnitude too strong for that to be the case.

3. (5^-) band at 2210.3 keV

The sequence of states beginning with the 2210.3 keV state shown on the extreme right of Fig. 1 has a regularity suggestive of a band, although it may be the case that the 5^- state is not the lowest member (band head) since the in-band transitions become less competitive at lower spins and intensity is inevitably transferred out of the band.

The moment of inertia implied by the relative energy plot in Fig. 8 is similar to that of the 8^- band (discussed in the following subsection) and also to that of the possible 6^- sequence (right of Fig. 2). The properties of these two sequences are similar to the signature-split 5^- band in the isotone ^{184}Pt assigned to the $\nu(i_{13/2}^{-1}\, p_{3/2}^{-1})$ prolate configuration [46]. The alignments of both bands (extracted using the same reference) are shown in Fig. 10 where some similarity is apparent, although the bands are certainly not identical.

4. $K^\pi = 8^-$; prolate configuration

The alignment of the 8^- band is essentially the same as in the 8^- bands in the (prolate-deformed) $N=106$ isotones except for local perturbations at spin 13^-. The magnitude of the alignment is consistent with the presence of the $9/2^+[624]$ orbital in the configuration, while the $(g_K - g_R)$ values obtained from the in-band branching ratios (Table IV) give an average of $-0.182(18)$ which agrees with the value of $-0.194(6)$ in ^{184}Pt (deduced in Ref. [47] from the data of Carpenter *et al.* [46]) and the expected value for the two-quasineutron configuration of $-0.3(1)$, where the error is largely due to the uncertainty in g_R. The sign comes from the large negative anisotropy observed for the in-band transitions, required if the sign of the quadrupole moment is positive as expected for prolate deformation. These results agree with the configuration-constrained PES calculations of Xu *et al.* [41] which predict that the prolate minima will have deformations of similar magnitude for the 8^- configurations in ^{184}Pt, ^{186}Hg, and ^{188}Pb and with neglible gamma asymmetry but with some softness in the gamma direction [41]. As stated earlier, the *K*-hindrance factors are consistent with predominantly good-*K*.

B. Non-yrast low-spin states

Although the decay of the 8^- isomer is complicated, the fragmentation results in the identification of a number of low-spin states and sequences. These include possible band structures such as the sequence beginning either at the 1219 keV (1^-) state or the 1516.6 keV 3^- state; the sequence associated with the 1787.9 keV, 5^+ state and the sequence associated with the 952.5 keV, 2^+ state.

Judging from Fig. 8, if interpreted as members of a band, the negative parity states would have a moment of inertia similar to those of the oblate structures. However, no deformed two-quasiparticle structures (the lowest of which are of two-quasineutron characters) would be expected so low in energy. Hence, this sequence and the other states are likely to be either from spherical configurations or from vibrational and rotational bands based on the effective ground states of each deformed minimum.

The same line of reasoning applies to the odd-spin positive parity states (5^+ state at 1788 keV, 7^+ state at 2217 keV), which must be candidates for states of a γ band. (Note also that the 1411 keV state which has a tentative 4^+ assignment would coincide with the expected energy of a 3^+ state if one were to extrapolate from above.) There is limited information about such bands in this region and it should be remembered that in simple terms, such vibrations could arise from each minimum, leading to a complex situation. For example, Delarouche *et al.* [48] analyze the evidence for γ-vibrational states in a range of Hg nuclei where shape coexistence is present, including the isotone ^{186}Hg. They identify a number of states, including for example, 2^+, (3^+), (5^+), and (7^+) states at 1096, 1433, 1868, and 2428 keV, which they characterize as candidates for γ-vibrational states of a perturbed structure. These do not match directly with states in ^{188}Pb but there are some similarities in the observed structures. The authors carry out extensive calculations using the generator coordinate method with the Gogny force and a parameter-free collective Hamiltonian which predict complex spectra, which match in a limited fashion, the experimental data.

Similarly in the isotone ^{184}Pt in which there is evidence for shape coexistence, decay measurements indicate a complex level scheme including the expected (coexisting) 0^+ bands, and also several $K^\pi = 2^+$ bands, at low energy, with strong $E0$ transitions in between [49]. Neither the origin of the band structures nor the complicated branches between them have been reproduced in detail, although the implication is that they arise, at least in part, from γ vibrations in each of the coexisting wells.

1. Negative-parity two-neutron-hole states

Spherical configurations can also mimic band structures, hence some caution is needed in making such assignments. Pomar *et al.* [50] discuss the systematics of negative parity two-neutron hole states in the light Pb isotopes in the framework of a combined quasiparticle shell-model calculation. The states expected at low energy arise from the multiplets associated with different combinations of the $i^{-1}_{13/2}$ neutron hole with the $p^{-1}_{3/2}$, $f^{-1}_{5/2}$, $f^{-1}_{7/2}$, and $h^{-1}_{9/2}$ neutron holes. From their calculations of relative single-particle energies, consideration of the multiplet structures and the residual interactions, and the systematics, one would expect, in order of excitation energy, a 3^- state from the $i^{-1}_{13/2} \otimes f^{-1}_{7/2}$ configuration, a 5^- state from the $i^{-1}_{13/2} \otimes p^{-1}_{3/2}$ configuration, and a 7^- state from a mixture of the $i^{-1}_{13/2} \otimes f^{-1}_{7/2}$ configuration and the $i^{-1}_{13/2} \otimes p^{-1}_{3/2}$ configurations. There are several ways of producing a 9^- state and the maximum spin state would be an 11^- state from the $i^{-1}_{13/2} \otimes f^{-1}_{h/2}$ configuration. The 1517.6 keV (3^-), 1955.9 keV (5^-), and 2474.0 keV (7^-) states are obvious candidates for association with these spherical states, rather than with a collective band (see above), and their energies fit smoothly into the systematics of the negative-parity states in the heavier isotopes. The 11^- state would be expected about 1 MeV above the 5^- state, and this could be the state at 3183.2 keV that perturbs the 11^- state of the 8^- band.

2. Band-mixing results

Our band-mixing results reported previously [21] corresponded to fits which included the new non-yrast states identified here, and also the two excited 0^+ states known at the time.

As discussed earlier, the most recent measurements give a new value of 588 keV for the $0^{+\prime}$ state, but they have not confirmed the presence of the second excited 0^+ state. We have therefore carried out further calculations adopting 588 keV for the $0^{+\prime}$ state energy and without a $0^{+\prime\prime}$ state. A number of solutions are possible in these fits, depending on how the band parameters, etc., are constrained, and not all can be discussed here. For illustration, in the lower panels of Fig. 11 we show the refit, and some representative results where different assumptions about the interactions and energies of the unperturbed spherical sequence are made. In Fig. 11(a) these energies are described by a weakly deformed rotor, whereas in Figs. 11(b) and 11(c) they are taken to be

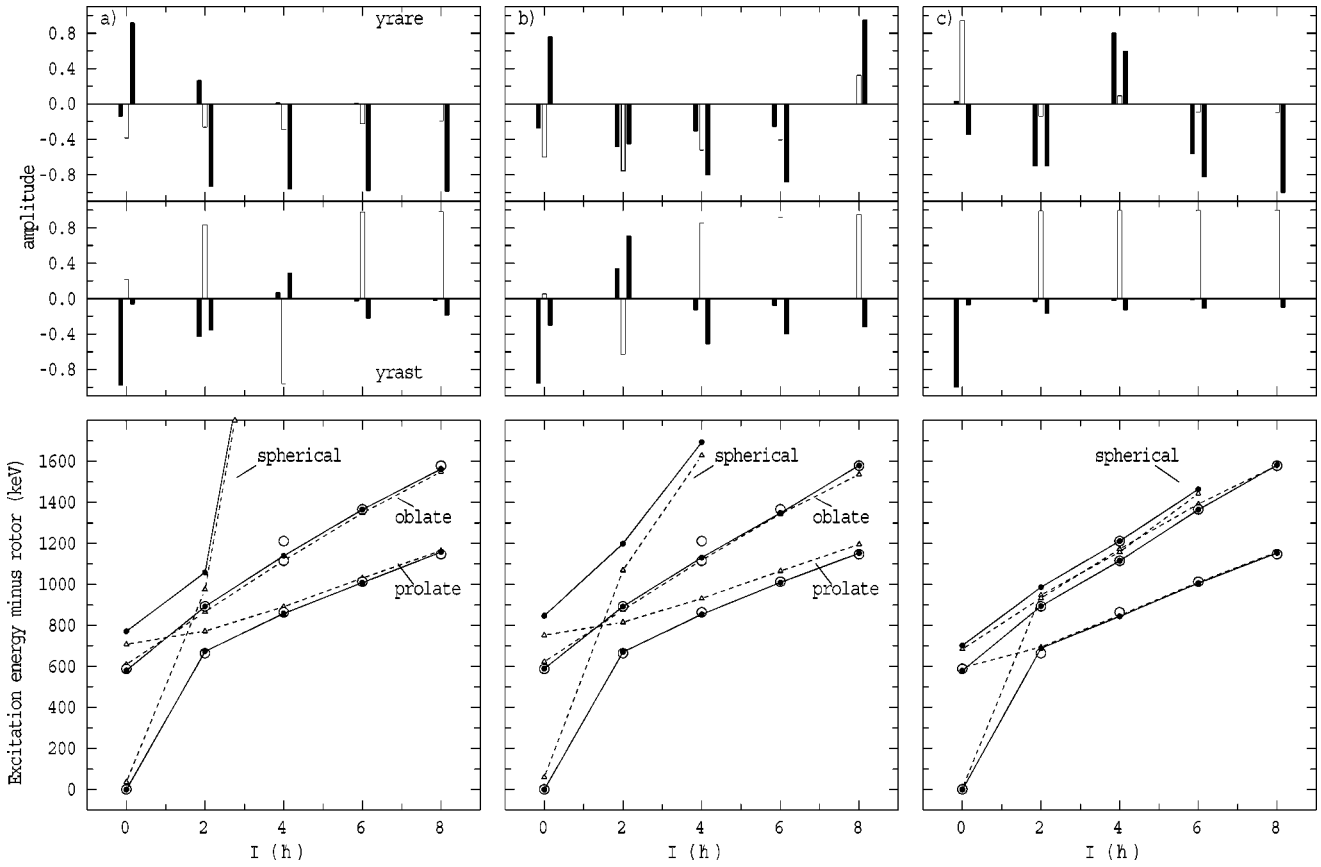

FIG. 11. Examples of three-state mixing calculations for ^{188}Pb with three sets of conditions (a), (b), and (c) as described in the text. The lower panels show the fits with experimental states as open circles. Dashed lines connect the unperturbed sequences, while the final states are indicated by filled circles connected by solid lines. Only the fit on the right includes the $4^{+\prime\prime}$ excited state. The upper panels give the amplitudes with three columns representing, from left to right, the spherical, prolate and oblate amplitudes.

similar to the spherical sequences in the heavier Pb isotopes where the deformed intruder bands are higher in energy. In (a) the three possible band interactions are included, whereas in (b) and (c) the interaction between the notionally spherical and prolate bands (V_{s-p}) is set to zero, in line with the suggestions of the IBM model calculations discussed earlier.

The upper panels of this figure show the calculated amplitudes for the spherical, prolate, and oblate components (three columns in that order) for the fitted yrast and yrare states, as a function of spin.

The main difficulty in these calculations is the uncertainty in the energies of the unperturbed spherical states and the limited number of experimental states known, particularly with the new uncertainty in the existence of a second excited 0^+ state.

The calculated widths and total decay branches predicted from calculation (a) are similar to those we reported previously [21]. The experimental and predicted ratios are compared in Table VI and in Fig. 12. In this calculation all interactions were included, with the fit requiring $V_{s-p}=90$ keV, $V_{s-o}=-70$ keV, $V_{o-p}=70$ keV. The $E0$ branches are reasonably well predicted, but the $\Gamma_e(E0)/\Gamma_\gamma(E2)$ ratios for the $J \rightarrow J$ transitions are overestimated. That discrepancy can be traced directly to an underestimate of the $\Gamma_\gamma(E2)$ value. Overall, the $E2$ branching ratios for all transitions are reasonably well reproduced, except for the two strongest transitions from the $4^{+\prime}$ state where the out-of-band $E2$ transition to the yrast 2^+ state is underestimated. This could be a limitation of using spin-independent interactions, since better results are obtained for the $4^{+\prime}$ branching if a large interaction is used to produce more mixing, but that interaction produces too much mixing and consequently branching at higher spins. It is plausible that the potential barriers could be less well defined at low spins, implying an interaction which reduces with spin. (In the following section the possibility of $K=2$ mixing from the γ band is outlined, and such mixing could result in $M1$ components in the $J \rightarrow J$ transitions and therefore an increase in the Γ_γ widths for these transitions.)

The calculation shown in Fig. 11(b) is a fit to the known yrast and yrare experimental states assuming the unperturbed 2^+ spherical state lies above both oblate and prolate unperturbed 2^+ states, as is the case in (a). With $V_{s-p}=0$, a comparable fit is obtained but with relatively large values of 190 and 130 keV for spherical-oblate (V_{s-o}) and oblate-prolate interactions (V_{o-p}), respectively. The unperturbed moment-of-inertia parameters, which translate to quadrupole moments magnitudes of 6.2 and 3.4 eb for the unperturbed prolate and oblate bands are similar to those of (a). The position of the $0^{+\prime}$ state is reproduced and the $0^{+\prime\prime}$ state is predicted to lie at 847 keV. The γ-ray branching ratios calculated from

TABLE VI. Predicted decay widths and branching ratios of selected nonyrast and yrast states in ^{188}Pb from a representative band-mixing calculation [calculation (a) in the text].

Initial state	I_i^π	I_f^π	$M\lambda$	E_γ (keV)	Γ_γ (10^{-5} eV)	Γ_e (10^{-5} eV)	Theo. %	Exp. %
2299	$8^{+\prime}$	6^+	$E2$	866	1.90	0.017	15.8	6(2)
		$6^{+\prime}$	$E2$	513	9.63	0.284	81.4	75(5)
		8^+	$E2$	432	0.065	0.003	0.6	15(2)
		8^+	$E0$			0.273	2.2	3.7(6)
1786	$6^{+\prime}$	4^+	$E2$	723	0.63	0.008	9.6	10(3)
		$4^{+\prime}$	$E2$	472	5.46	0.211	84.6	79(4)
		6^+	$E2$	353	0.04	0.003	0.7	5(1)
		6^+	$E0$			0.339	5.1	6(1)
1315	$4^{+\prime}$	2^+	$E2$	592	0.24	0.004	7.4	39(3)
		$2^{+\prime}$	$E2$	362	2.31	0.130	75.9	43(2)
		$2^{+\prime\prime}$	$E2$	206	0.017	0.005	0.7	–
		4^+	$E2$	251	0.021	0.003	0.7	6(1)
		4^+	$E0$			0.489	15.3	10(1)
953	$2^{+\prime}$	0^+	$E2$	953	1.06	0.008	56.5	68(2)
		$0^{+\prime}$	$E2$	365[a]	0.57	0.036	32.4	$\leqslant 3$
		$0^{+\prime\prime}$	$E2$	183[b]	0.02	0.013	1.9	$\leqslant 5$
		2^+	$E2$	229	0.001	0.0003	0.1	8(1)
		2^+	$E0$			0.176	9.3	16(2)
1433	6^+	4^+	$E2$	370	6.11	0.386	99.97	100
1064	4^+	2^+	$E2$	340	2.65	0.220	99.98	100
724	2^+	0^+	$E2$	724	5.92	0.076	99.65	100
580[c]	$0^{+\prime}$	0^+	$E0$			0.192	100	
770[d]	$0^{+\prime\prime}$	0^+	$E0$			0.884	56.3	
	$0^{+\prime\prime}$	$0^{+\prime}$	$E0$			0.619	39.4	
	$0^{+\prime\prime}$	2^+	$E2$[e]			0.066	4.2	

[a]Expected energies for the $0^{+\prime}$ state at 588 keV.
[b]Predicted $0^{+\prime\prime}$ at 770 keV.
[c]For the $E0$ components in $J\rightarrow J$ transitions, the width depends on the assumption that $K=0$ in initial and final states.
[d]Calculated energies.
[e]Because of its low energy (49 keV) the γ-ray branch is negligible.

the mixed wave functions do not agree as well with experiment, but they are reasonable. A persistent problem, however, is that the predicted branching from the $4^{+\prime}$ state (at 1315 keV) is $\sim$90% to the $2^{+\prime}$ state, whereas experimentally approximately 40% goes via the 592 keV transition to the 2^+ yrast state. We have not found, in any of these fits, a solution to this discrepancy that does not also compromise the agreement in the branching of the higher-spin states.

The calculation in Fig. 11(c) is a fit that includes the 1411 keV state, which is a candidate for the $4^{+\prime\prime}$ state. To reproduce experiments with this state included, it is necessary to rescale the unperturbed spherical sequence to be considerably more compressed than that used in the other calculation, and the interactions favored are much smaller with $V_{s-o}=46$ keV and $V_{o-p}\sim 0$. This fit is reasonable as far as energy reproduction is concerned although the 2^+ energy is overestimated by about 20 keV, but the calculated branching ratios disagree with experiment. The yrast 2^+ state, for example, is predicted to decay predominantly to the $0^{+\prime}$ state whereas it decays essentially 100% to the ground state. Examination of the wave functions shows that the difference between the two calculations is that the 2^+ state and the $0^{+\prime}$ are both predominantly prolate in the case of the calculation (c), whereas in the calculation (a) and (b), the order of the unperturbed oblate and prolate band heads is inverted, and both 2^+ and $0^{+\prime}$ states are highly mixed, with signs and amplitudes such that destructive interference occurs for this transition.

These results underline the importance of identifying the non-yrast states to act as constraints in the fitting, a situation now exacerbated by the uncertainty in the excited 0^+ states. Further, to distinguish between the effects of interference and incorrect magnitude of mixed amplitudes, it is necessary to have absolute as well as relative transition rates.

Other transitions of specific interest are possible branches from the $2^{+\prime}$ state to the excited 0^+ states which would provide a confirmation of the 0^+ state energies. Although in the calculation shown in Table VI a significant branch (32%) is predicted for the decay of the 953 keV $2^{+\prime}$ state to the $0^{+\prime}$ state, this branch is very sensitive to the fit parameters and,

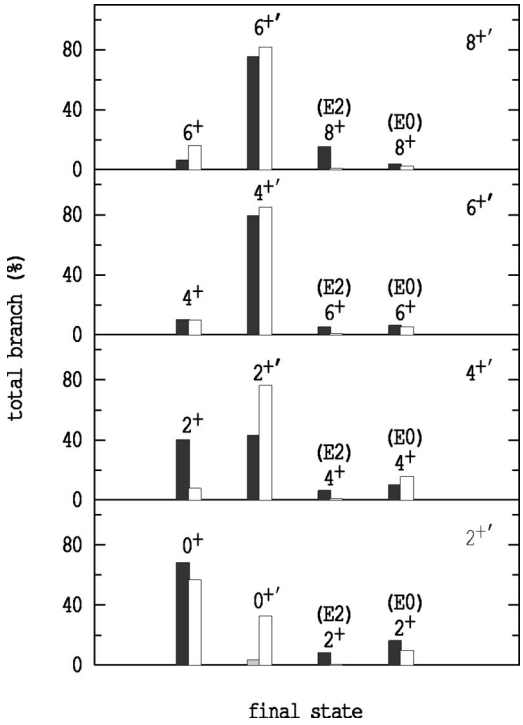

FIG. 12. Calculated (open columns) and experimental (filled) total branching ratios in ^{188}Pb for decays from yrare states as indicated in each panel. The shaded column for the $2^{+\prime}$ to $0^{+\prime}$ decay represents the experimental limit.

in any case, no significant branch has been observed. We give experimental limits of a few percent of the main transition to ground.

$E0$ strengths are often catalogued in terms of $\rho^2\times 1000$ for comparison. The widths given in Table VI correspond to values for $\rho^2\times 1000$ of approximately 7 and 25 for the $0^{+\prime}$ and $0^{+\prime\prime}$ decays, and 10, 27, 16, and 12 for the $2^{+\prime}$, $4^{+\prime}$, $6^{+\prime}$, and $8^{+\prime}$, $J\rightarrow J$ $E0$ components, respectively. These are of similar magnitude to those observed in other regions where shape coexistence is observed and attributed to mixing between states of moderately different deformation [51].

3. Low-spin state lifetimes

Very recently, lifetime measurements for the 2^+ and 4^+ yrast states were reported by Dewald *et al.* [52]. The results are limited, and not of high precision, but in principle they could be used to test the band mixing described above. The values reported in Ref. [52] are 13(7) ps for the 724 keV level and 16(8) ps for the 1064 keV levels. The decay widths calculated for these states in the present model are not very sensitive to different band-mixing alternatives, and for the widths given in Table VI, they translate to lifetimes of 11 ps and 23 ps for the yrast 2^+ and 4^+ states, respectively. These are consistent with the recent experiments, but at present, the experimental results are not accurate enough to significantly test the predictions.

The lifetimes predicted for the excited 0^+ states from decay widths given in Table VI are 343 ps and 42 ps for the $0^{+\prime}$ and $0^{+\prime\prime}$ states, respectively.

4. Four-band mixing and the γ band

As discussed previously, the 5^+ and 7^+ states at 1788 and 2217 keV are candidates for members of a γ band, with a possible 3^+ state at 1411 keV. The even-spin states of such a band could mix with the $K=0$ bands considered so far, with resultant $K=2$ admixtures. (The even spin states which originated from the γ band would thus be pushed up in energy.) We have extended the band mixing to include a fourth band. In the absence of other odd-spin positive parity states, the odd-spin states would be unperturbed, hence the unperturbed band properties, moment of inertia and band-head energy can be fixed from the experiment. This is an advantage, in terms of limiting the parameters. However, the introduction of a fourth band means that the number of possible interactions is increased. Without further model constraints, and preferably more experimental constraints through the identification of the perturbed even-spin states, it is not appropriate to place too much reliance on the fits at this stage. Nevertheless, the experimental states can be well reproduced, with inclusion of a γ band originating at 1238 keV. As indicated above, the resultant mixing of the even-spin members of such a band provides a mechanism for introducing $K=2$ admixtures into the $K=0$ bands, the main effect of which is to enable $M1$ components in the $J\rightarrow J$ transitions. Our preliminary evaluation of these suggests that they are not particularly significant, partly because both the intrinsic $M1$ matrix elements and the Clebsch-Gordan coefficients governing such transitions are relatively small. These are aspects which could in the future be addressed with the measurement of mixing ratios and direct conversion coefficients.

C. Comments on other theoretical approaches

Such phenomenological models contrast with the extensive but challenging microscopic approaches. The complexity of the energy surface for the Pb isotopes, however, and the difficulty of isolating different minima in PES calculations has led to the use of approximations to effectively constrain the potential for specific configurations [7]. The inclusion of dynamical effects would clearly be important in this situation, but this has not generally been achieved. Chasman, Egido, and Robledo [53] emphasized the difficulties of establishing orthogonality between the wave functions of the 0^+ states, in particular, given the low and uncertain potential barriers separating poorly defined minima. They carried out Hartree-Fock-Bogoliubov calculations with the Gogny force and explicit inclusion of configuration interactions, and also with a many-body variational approach. Their calculations predict the existence of three 0^+ states of different (but not precisely defined) deformation in a range of Pb nuclei from $A=182$ to $A=190$, but the results are sensitive to assumptions about degrees of freedom, such as the form and the strength of the pairing, and to the alternative calculational methods. Significant differences between theory and the limited experimental information available are apparent.

Theoretically it seems that calculations which include angular momentum projection may be required to produce a realistic configuration separation [54,55] at all spins. Very recent calculations by Bender *et al.* [56] have taken a signifi-

cant step towards this goal with extensive modeling of collective excitations in the isotopes $^{182-194}$Pb incorporating configuration mixing of angular-momentum-projected and particle-number-projected self-consistent mean-field states, with a Skyrme interaction and a density-dependent zero-range pairing force. These calculations obtain qualitative agreement for energy spectra and $E0$ and $E2$ transition rates (including some branching ratios in ^{188}Pb), but they still do not match experiment.

The results are illuminating in that they produce detailed wave functions in deformation space, showing directly the contributions from oblate, prolate, and spherical components. These (and others) are mixed in a complicated fashion, but they support, in a general way, the concept of shape coexistence. The main discrepancies for ^{188}Pb in particular are that the (mixed) oblate and prolate bands are calculated to lie in the opposite order from that observed in experiment, reflecting to some extent the failure of the theory to reproduce the relative-energy systematics through the isotopes, and they do not reproduce the spin-dependence of the ratio of $E0/E2$ widths deduced from the present work. A much faster fall off is predicted in theory, where the value for the $2^{+\prime}$ decay is within a factor of about 3 but the higher spin states become orders of magnitude smaller than observed. This is not surprising given that the experimental energy separation between the oblate and prolate bands, and implicitly therefore, the mixing, is not reproduced.

VIII. SUMMARY AND CONCLUSIONS

A detailed level scheme for ^{188}Pb has been established. It includes identification of excited states above the previously proposed 11^-, 12^+, and 8^- isomers whose properties have now been defined. A higher lying isomer with probable spin and parity 19^- has also been placed, and collective sequences above the 11^- and 8^- intrinsic states have been characterized. These and other two-quasiparticle excitations have been discussed in terms of the expected configurations of excitations within the proposed spherical, oblate, and prolate minima due to shape coexistence. Other non-yrast states including candidates for the oblate band, which interferes with the prolate yrast band, at low spin and excitation energy, have also been identified, and at least partly characterized. Their properties have been compared with the results of fits using three-band mixing constrained by the observed energies of the yrast and newly identified non-yrast states. The mixed wave functions extracted from these calculations are partly successful in describing the observed $E0$ and $E2$ branching ratios, but significant discrepancies remain. This is not surprising given the implicit assumptions of fixed deformation and spin-independent interactions, which may be questionable at the lowest spins. The value of further explorations with such models will depend on the identification or at least firm characterization of non-yrast states such as the expected $0^{+\prime\prime}$, $2^{+\prime\prime}$, and $4^{+\prime\prime}$ states, in order to firmly constrain the fits, and allow reliable extraction of parameters. Despite these limitations, the observed states and properties are largely consistent with the excitations expected of a nucleus which exhibits the coexistence of three different shapes.

ACKNOWLEDGMENTS

We thank Bob Turkentine for producing the targets, members of the Surrey group for assistance with the data collection, and the staff of the 88-in. cyclotron facility. G.D.D., A.P.B., and A.M.B. acknowledge the financial support of the Access to Major Facilities Program, administered by A.N.S.T.O.; Project No. = 2000/2001-H-04.

[1] J. Heese *et al.*, Phys. Lett. B **302**, 390 (1993).
[2] J. Bonn, G. Huber, H.-J Kluge, L. Kugler, and E. W. Otten, Phys. Lett. **38**, 308 (1972).
[3] J. Bonn, G. Huber, H.-J Kluge, and E. W. Otten, Z. Phys. A **276**, 203 (1976).
[4] J. L. Wood *et al.*, Phys. Rep. **215**, 101 (1992).
[5] F. G. Kondev *et al.*, Phys. Rev. C **62**, 044305 (2000).
[6] F. R. May, V. V. Pashkevich, and S. Frauendorf, Phys. Lett. **68B**, 113 (1977).
[7] R. Bengtsson and W. Nazarewicz, Z. Phys. A **334**, 269 (1989).
[8] W. Nazarewicz, Phys. Lett. B **305**, 195 (1993).
[9] G. D. Dracoulis, A. P. Byrne, and A. M. Baxter, Phys. Lett. B **432**, 37 (1998).
[10] G. D. Dracoulis *et al.*, Phys. Rev. C **60**, 014303 (1999).
[11] R. Julin, K. Helariutta, and M. Muikku, J. Phys. G **27**, R109 (2001).
[12] G. D. Dracoulis, Phys. Scr. **88**, 54 (2000).
[13] A. N. Andreyev *et al.*, Nature (London) **405**, 430 (2000).
[14] A. M. Baxter, A. P. Byrne, G. D. Dracoulis, R. V. F. Janssens, I. G. Bearden, R. G. Henry, D. Nisius, C. N. Davids, T. L. Khoo, T. Lauritsen, H. Penttila, D. J. Henderson, and M. P. Carpenter, Phys. Rev. C **48**, R2140 (1993).
[15] W. Reviol, C. J. Chiara, O. Pecheneya, D. G. Sarantites, P. Fallon, and A. O. Macchiavelli, Phys. Rev. C **68**, 054317 (2003).
[16] P. Van Duppen, E. Coenen, K. Deneffe, M. Huyse, and J. L. Wood, Phys. Lett. **154B**, 354 (1985).
[17] P. Dendooven, P. Decrock, M. Huyse, G. Reusen, P. Van Duppen, and J. Wauters, Phys. Lett. B **226**, 27 (1989).
[18] R. G. Allat *et al.*, Phys. Lett. B **437**, 29 (1998).
[19] G. D. Dracoulis, Meeting on "Shape Mixing, and Modifications in the Nuclear Mean Field with Applications to the Pb-region," Gent, 2001 (unpublished).
[20] G. D. Dracoulis, A. P. Byrne, G. J. Lane, A. M. Baxter, T. Kibédi, A. O. Macchiavelli, P. Fallon, and R. M. Clark, in *Proceedings of the Conference on Frontiers of Nuclear Structure*, edited by P. Fallon and R. Clark, AIP Conf. Proc. No. 656 (AIP, Melville, NY, 2003).
[21] G. D. Dracoulis, A. P. Byrne, G. J. Lane, A. M. Baxter, T. Kibédi, A. O. Macchiavelli, P. Fallon, and R. M. Clark, Phys. Rev. C **67**, 051301(R) (2003).
[22] M. Cromaz, T. J. M. Symons, G. J. Lane, I. Y. Lee, and R. W. MacLeod, Nucl. Instrum. Methods Phys. Res. A **462**, 519 (2001).

[23] F. Rösel *et al.*, At. Data Nucl. Data Tables **21**, 291 (1978).
[24] Y. Le Coz *et al.*, EPJdirect **3**, 1 (1999).
[25] N. Bijnens *et al.*, Z. Phys. A **356**, 3 (1996).
[26] A. Andreyev *et al.*, J. Phys. G **25**, 835 (1999).
[27] A. Andreyev *et al.* (private communication, 2002).
[28] K. Van de Vel *et al.*, Phys. Rev. C **68**, 054311 (2003).
[29] G. D. Dracoulis, Phys. Rev. C **49**, 3324 (1994).
[30] P. Van Duppen, E. Coenen, K. Deneffe, M. Huyse, and J. L. Wood, Phys. Rev. C **35**, 1861 (1987).
[31] P. Van Duppen, M. Huyse, and J. L. Wood, J. Phys. G **16**, 441 (1990).
[32] D. S. Delion, A. Florescu, M. Huyse, J. Wauters, P. Van Duppen, ISOLDE Collaboration, A. Insolia, and R. J. Liotta, Phys. Rev. C **54**, 1169 (1996).
[33] T. Kibédi, G. D. Dracoulis, A. P. Byrne, P. M. Davidson, and S. Kuyucak, Nucl. Phys. **A567**, 183 (1994).
[34] R. Fossion, K. Heyde, G. Thiamova, and P. Van Isacker, Phys. Rev. C **67**, 024306 (2003).
[35] K. Heyde and R. A. Meyer, Phys. Rev. C **42**, 790 (1990).
[36] H. Mach, M. Moszynski, R. L. Gill, G. Molnar, F. K. Wohn, J. A. Winger, and J. C. Hill, Phys. Rev. C **42**, 793 (1990).
[37] C. Y. Wu, H. Hua, and D. Cline, Phys. Lett. B **541**, 59 (2002).
[38] P. M. Walker, G. D. Dracoulis, A. P. Byrne, B. Fabricius, T. Kibédi, A. E. Stuchbery, and N. Rowley, Nucl. Phys. **A568**, 397 (1994).
[39] W. Nazarewicz, M. A Riley, and J. D. Garrett, Nucl. Phys. **A512**, 61 (1990).
[40] Xu Fu-Rong, Chin. Phys. Lett. **18**, 750 (2001).
[41] F. R. Xu, P. M. Walker, and R. Wyss, Phys. Rev. C **59**, 731 (1999).
[42] F. R. Xu, P. M. Walker, J. A. Sheikh, and R. Wyss, Phys. Lett. B **435**, 257 (1998).
[43] A. J. M. Plompen *et al.*, Nucl. Phys. **A562**, 61 (1993).
[44] G. J. Lane, G. D. Dracoulis, A. P. Byrne, P. M. Walker, A. M. Baxter, J. A. Sheikh, and W. Nazarewicz, Nucl. Phys. **A586**, 316 (1995).
[45] N. A. Smirnova, P.-H. Heenen, and G. Neyens, Phys. Lett. B **569**, 151 (2003).
[46] M. P. Carpenter *et al.*, Nucl. Phys. **A513**, 125 (1990).
[47] M. P. Robinson, A. E. Stuchbery, R. A. Bark, A. P. Byrne, G. D. Dracoulis, S. M. Mullins, and A. M. Baxter, Phys. Lett. B **530**, 74 (2002).
[48] J. P. Delarouche *et al.*, Phys. Rev. C **50**, 2332 (1994).
[49] Y. Xu, K. S. Krane, M. A. Gummin, M. Jarrio, J. L. Wood, E. F. Zganjar, and H. K. Carter, Phys. Rev. Lett. **68**, 3853 (1992).
[50] C. Pomar, J. Blomqvist, R. J. Liotta, and A. Insolia, Nucl. Phys. **A515**, 381 (1990).
[51] J. L. Wood, E. F. Zganjar, C. De Coster, and K. Heyde, Nucl. Phys. **A651**, 323 (1999).
[52] A. Dewald *et al.*, Phys. Rev. C **68**, 034314 (2003).
[53] R. R. Chasman, J. L. Egido, and L. M. Robledo, Phys. Lett. B **513**, 325 (2001).
[54] R. R. Rodriguez-Guzman, J. L. Egido, and L. M. Robledo, in *Proceedings of the Conference on Frontiers of Nuclear Structure*, edited by P. Fallon and R. Clark, AIP Conf. Proc. No. 656 (AIP, Melville, NY, 2003). p. 303.
[55] T. Duguet, M. Bender, P. Bonche, and P.-H Heenen, Phys. Lett. B **559**, 201 (2003).
[56] M. Bender, P. Bonche, T. Duguet, and P.-H Heenen, Phys. Rev. C (to be published).